REPORT DOCUMENTATION PAGE

Form Approved
OMB No. 0704-0188

1. REPORT DATE *(DD-MM-YYYY)*	2. REPORT TYPE	3. DATES COVERED *(From - To)*
07/20/2006	Final Performance Report	9/1/05 - 4/30/06

4. TITLE AND SUBTITLE
Nanoscale Polymeric Photocells by Advanced Electrospinning

5a. CONTRACT NUMBER

5b. GRANT NUMBER
F49620-03-1-0164

5c. PROGRAM ELEMENT NUMBER

6. AUTHOR(S)
PI: Dr. Anvar Zakhidov
Co-PI: Dr. John Ferraris and Dr. Kenneth Balkus

5d. PROJECT NUMBER

5e. TASK NUMBER

5f. WORK UNIT NUMBER

7. PERFORMING ORGANIZATION NAME(S) AND ADDRESS(ES)
The University of Texas at
Dallas
2601 North Floyd Road, BE26
Richardson, TX 75080

8. PERFORMING ORGANIZATION REPORT NUMBER

9. SPONSORING / MONITORING AGENCY NAME(S) AND ADDRESS(ES)
AFOSR
875 North Randolph Street
Suite 325, Room 3112
Arlington, VA 22203
Dr. Charles Lee

10. SPONSOR/MONITOR'S ACRONYM(S)
AFOSR

11. SPONSOR/MONITOR'S REPORT

AFRL-SR-AR-TR-06-0341

12. DISTRIBUTION / AVAILABILITY STATEMENT
Approve for Public Release: Distribution Unlimited

13. SUPPLEMENTARY NOTES
None

14. ABSTRACT We presented detailed study of postproduction heat treatment of organic solar cells based on RR-P3HT:PCBM composite in a wide temperature range. The efficiency of such device was significantly improved by postproduction heat treatment. Optimized parameters yielded >3% efficiency for devices on glass substrates and of ≤3% for that on flexible substrates.
We also report studies of nanocomposites of conjugated polymer with infrared-sensitive, PbSe NCs. Thin film cells show good diode characteristics and sizable photovoltaic response with an open circuit voltage, V_{oc}, of ~ 0.3-0.4 V, short circuit currents, J_{sc}, of ~ 0.2 mA/cm^2. Photovoltaic response is observed as far to the red as 2 microns, which is desirable for efficient utilization of both infrared and ultraviolet regions of the solar spectrum.
We have demonstrated that MWCNT sheet can be used as the hole collecting electrode in organic solar cells based on RR-P3HT : PCBM composites. Our preliminary results show relatively high photovoltaic characteristics with an open circuit voltage of 0.49V, a short circuit current of 5.47 mA/cm^2 and efficiency of 1.3%.
Novel polymers are synthesized, including Donor/Acceptor block copolymers and functionalized PHT. Their optical and electric properties were characterized, and we started testing their application in both photovoltaic cells and photodetectors.

15. SUBJECT TERMS

16. SECURITY CLASSIFICATION OF:			17. LIMITATION OF ABSTRACT	18. NUMBER OF PAGES	19a. NAME OF RESPONSIBLE PERSON
a. REPORT	b. ABSTRACT	c. THIS PAGE	UU or SAR	52	Dr. Anvar Zakhidov
					19b. TELEPHONE NUMBER *(include area code)* 972-883-6218

Standard Form 298 (Rev. 8-98)
Prescribed by ANSI Std. Z39.18

Final Performance Report for the AFOSR program F49620-03-1-0164

PI name: Dr. A.A. Zakhidov

Institution: University of Texas at Dallas

Address: P.O. Box 830688, M/S: BE 26
Richardson, TX 75083-0688

Agreement number: F49620-03-1-0164

Date: July 20, 2006

Table of contents

Objectives

Main goal: to create high efficiency ($\eta > 5$ %) flexible solar cells on plastic substrates, based on a combination of either conjugated polymers (regioregular polyahexylthiophenes and functionalized polyhexylthiophene) with organic small molecules C60 (or PCBM), or with inorganic nanoparticels (infrared nanocrystals, Carbon nanotubes or TiO2 nanofibers).

New objectives: Since we experienced problems with nanofibers of TiO_2 by electrospinning method (small yield and large diameter of nanofibers, inability to incorporate long fibers into the thin film architecture), we started working on another inorganic components: nanocrystals (PbS, PbSe) in which the process of charge multiplication can be a novel method of efficiency increase. Using carbon nanotubes as transparent electrodes was another new target.

Status of effort

- The first year of the project we created the nanofibers of various polymers and titania by advanced electrospinning, and this activity is described in detail in our progress reports. However due to spatially bulky geometry of electrospun fibers, the use of such nanofibers in thin film type solar devices was not very promising, due to inability to deposit charge collecting electrodes. Therefore we switched to different ways of polymeric thin film deposition (by spin coating, etc.) while keeping the carbon nanotubes as a key hybrid component of the architecture.

- During the second and third year of the project we performed fabrication and the detailed study of organic solar cells based on RR-P3HT:PCBM composite in a wide temperature range of post-annealing from 75 °C to 150 °C. The efficiency of the photovoltaic device was significantly improved by postproduction heat treatment. The optimal phase separation of PCBM and RR-P3HT into bi-continuous network structure occurs within very short period of time and is very stable. We found that the optimal concentration of PCBM in RR-P3HT matrix is rather low, only 34 w.%

  For solar cells on glass the best parameters were obtained after annealing at 90 °C for 3 min:

  U_{oc}=0.61V, J_{sc}=14.3 mA/cm^2, FF=0.35 and **η=3.05%.**

  The short circuit current density is linearly increasing with intensity indicating negligible bimolecular recombination in the device. FF decreases with increasing intensity. Efficiency reached a maximum 3% at 25 mW/cm^2 and then decreases to 2% at AM1.5 100 mW/cm^2. The efficiency can be improved significantly (over 20%) by using insertion of thin LiF layer between the organic active layer and the Al electrode and by using low resistance ITO (<10Ω/□).

  We have fabricated **flexible bulk-heterojunction solar cells** on flexible substrates (ITO coated PET, 30 Ω/sq. from Delta Technologies) using the optimized heat treatment parameters; We obtained the following parameters for the best device:

  U_{oc} = 0.59 V, J_{sc} = 9.32 mA/cm^2, FF = 0.49 and **η = 2.69%.**

- In the last year of this program we used the functional nanostructures: a) transparent carbon nanotube (CNT) sheets (developed by us), and b) low-gap quantum dots (NC) of PbSe in high efficiency solar cells architectures, which we have created in earlier years. Fundamental goal with PbSe NCs was to test the carrier multiplication phenomena (CM) in photovoltaic response.

Continuous efforts were endeavored in annealing optimized bulk heterojunctions (BHJ) of low and high molecular weight (MW) polymer (regioregular poly-hexyl-thiophene) mixtures with fullerene derivative PCBM, while we also started testing Graetzel dye sensitized cells geometries with CNT sheets as counterelectrodes.

Meanwhile we continue to explore methodologies for the fabrication of meoporous TiO_2 fibers. Application of these fibers in the present solar cell configuration requires nanofibers (<100nm). Ideally the electrospun fibers would have diameters <20nm in diameter. We have been exploring the controlled growth of porous TiO_2. While fibers in the 20nm range can be achieved the yield is quite low and may not prove competitive with a direct synthesis method. One of the more promising approaches is the molecular sieve templated growth of mesoporous TiO_2. In this case mesoporous silica such as DAMN-1 or SBA-15 is infiltrated with a TiO_2 precursor, generally $TiCl_4$. Upon hydrolysis and removal of the silica, a mesoporous TiO_2 should remain.

New families of polymers have been home synthesized for making D-A block copolymers. Chemically modify conducting polymers which bear some functional groups capable of incorporating with nanocrystals were synthesized for hybrid solar cells.

Accomplishments/New Findings

Part 1. Set up for solar cells fabrication and characterization as well as Advanced Electrospinning of Polymers and Titania Fibers

1.1 Brief introduction

During the first reporting period of the project (March to September 2003) we devoted to the following tasks:

1. Created the compete solar cells characterization set up, which allows testing of plastic solar cells in ambient or in dry box.

A lab dedicated to the characterization of these devices is in place in special bay in Clean Room Facility at UTD, with a senior physicist responsible for performing these measurements assisted by a team of trained graduate students. The capabilities include the determination of power efficiency under a variety of Air Mass (AM) conditions. AM 1.5 will be used as the standard illumination conditions for solar cells with intended terrestrial applications.

2. Two advanced electro spinning system are created and the fibers of conjugated polymers and of TiO2 are obtained, with diameters of the fibers in the range of 50-100 nm.
3. The prototypes of polymeric solar cells are created based on conjugated polymers bulk heterojunctions with fullerenes and PCBM C_{60} derivatives. After the annealing the energy efficiency is about 2 % on glass substrates.
4. New types of conjugated polymers of BEH-PPV family are synthesized, with D and A properties so that their D-A block-copolymers can be created. These polymers are being now characterized for photovoltaic applications.

Characterization of the organic solar cell device test structures in terms of a wide variety of parameters is critical to the determination of the progress of the project. Nanotech Institute, University of Texas at Dallas (UTD) has created full photovoltaic device characterization facilities and is experienced in making these crucial measurements. Typical efficiency measurements include both Current-Voltage (I-V) characteristics and photoreponsivity spectrum.

Current-Voltage (I-V) curves are now easily performed automatically using the home-developed LabView based program to determine the open-circuit voltage, short-circuit current, and device fill-factor, and the power efficiency will then subsequently be determined by equation (1).

$$\eta = V_{oc} I_{sc} FF / P \qquad (1)$$

This equation expresses the power efficiency as the ratio of useful power ($Voc\ I\,sc\ FF = Vmax\ Imax$) to the power of incoming light, which in a simple approximation is $P = Nh\omega$, with $h\omega$ being average energy of photon. Here fill factor FF describes internal losses due to the serial resistance of the device. In addition, each of these parameters will be measured as a function of time in order to determine the stability of the device both long and short-term. However, this formula does not explicitly reflect the physical processes which control V_{oc}, I_{sc} or FF, in such a way that one can systematically improve the efficiency by changing those steps in photogeneration and charge collection processes. We have

shown that starting with equation (1) the energy conversion efficiency η of organic photocells can be expressed as in equation (2) as a product of five terms, each corresponding to a physical step in the sequence of light transformation and having clear physical meaning, which can be improved.

$$\eta = \alpha(\omega) \cdot \Phi_{ex} \cdot \varphi_{e-h} \cdot \xi_{en} \cdot FF \qquad (2)$$

These parameters are (1) The efficiency of photon collection $\alpha(\omega)$; (2) the quantum efficiency of exciton dissociation Φ_{ex}, which reflects exciton diffusion to D-A interface followed by primary D-A charges separation as a coupled interfacial CT state; (3) the quantum yield φ_{e-h} of free electrons generation in A and free holes in D parts; (4) the energetic factor $\xi_{en}=eV_{oc}/h\nu$ which shows what part of absorbed photon energy can be converted into electrical energy; and (5) the fill factor which is usually high in insulating 2.e. undoped D or A organic systems, due to low mobility of carriers, and small dark concentration of carriers.

Each of these parameters, in addition to the net charge generation efficiency $\eta_{ch} = \alpha(\omega)\Phi_{ex}\varphi_{e-h}$ (which is a number of charges produced per each photon), can be measured and tuned to optimize device performance and they will be determined for fabricated device structures in order to more fully elucidate the physical mechanisms underlying device operation.

1.2 List of equipment, installed for AFOSR Flexible solar cells.

Device Fabrication Facilities in Clean Room

Special bay in Clean Room dedicated for Organic Devices including the following devices:

- Thin Film Deposition Vacuum Systems for Metal and Organic Deposition equipped with Sigma-Instruments Controllers for Automatic Co-deposition.
- Organic Purification System

Excess to other devices in Clean Room include E-beam and Photolithography Systems, Plasma Research Systems and E-beam Evaporation Systems.

Solar Cell Characterization Laboratory

- ThermoOriel Solar Simulator based on 150W Xe Ozone Free Arc Lamp Source with Air Mass Filters
- Spectral Complex based on Cornerstone 130 Motorized 1/8m Monochromator and 75W QTH Sources, UV-enhanced Calibrated Si-detector and 2W Thermopile Detector (Spectra-Physics).
- MBios Surface Profilometer XP1
- Alessi Probe Station and Keithely Semiconductor Parameter Characterization System 4200 and Keithley 590 CV analyzer.
- Physical Parameters Measurement Systems (PPMS, Quantum Design) and MPMS magneto-transport system with temperatures from 10 - 350 K and magnetic fields to 9 T equipped with optical fiber input.

Microscopy Laboratory

- Leo 1530 VP Field Emission Scanning Electron Microscope (FESEM) with variable pressure, EDAX, and e-beam nanolithography
- Zyvex NanoManipulator S-100
- Veeco/DI Nanoscope IV AFM/STM
- Olympus and Zeiss optical microscopes

Carbon Nanotube Synthetic Facilities

- Arc-chamber for advanced synthesis of single wall carbon nanotubes and fullerenes

– Two CVD furnaces for synthesis of multi- and single wall nanotubes

Electrospinning of conjugated polymers.

We have developed the apparatus and successfully have electrospun the nanofibers of a series of conjugated polymers and fabricated solar cell. Some examples of polymers nanofibers are shown below.

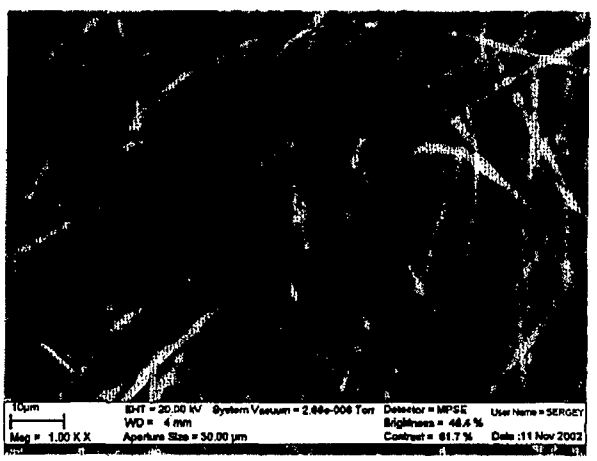

Figure 1.2.1 SEM image of PEO-MEH-PPV electrospun fibers.

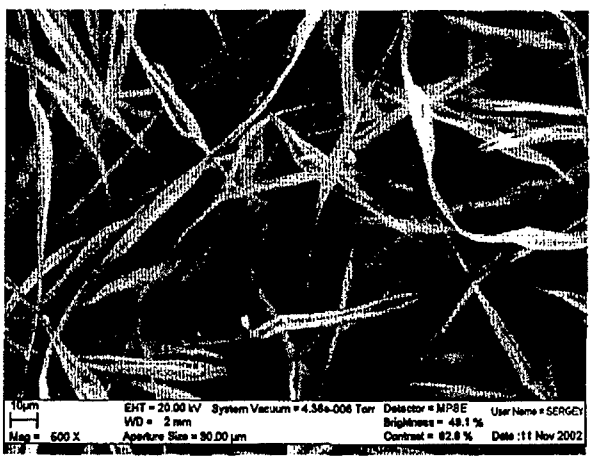

Figure 1.2.2 SEM image of PVK electrospun fibers.

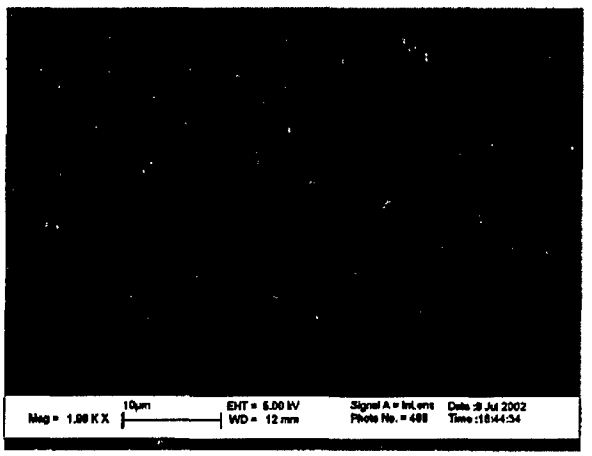

Figure 1.2.3 SEM image of PEO-Laser Carbon nanotube electrospun fibers.

Part 2. Optimization of Postproduction Heat Treatment for Fabrication of Highly Efficient Plastic Solar Cell

ABSTRACT

We report the detailed study of a postproduction heat treatment of flexible organic solar cells based on regio-regular (RR) P3HT:PCBM composite in a wide temperature range from 75 °C to 150 °C. The efficiency of the photovoltaic device was significantly improved by postproduction heat treatment and both optimal annealing temperature and time dependencies were determined. Optimized parameters yielded >3% efficiency for devices on glass substrates and, using these optimized parameters, an efficiency of ≤3% was found for devices fabricated on flexible substrates. The optimal phase separation of PCBM and RR-P3HT into a bi-continuous network structure occurs within a very short period of time and is very stable. We have found that the optimal concentration of PCBM in a RR-P3HT matrix is rather low, only 35 w.%. The effect of MW on the preproduction parameters and the postproduction treatment conditions has been extensively studied and we found that significant differences for the optimal temperature T_{opt} and the duration time t_{opt} as well as for other optimal pre- and post-production conditions for low- and high-MW P3HT/PCBM composite bulk heterojunction solar cells.

INTRODUCTION

Plastic solar cells have received considerable attention as low cost, low weight and mechanically flexible photo-voltaic devices after the introduction of the concepts of a bulk-heterojunction and a bi-continuous interpenetrating network of acceptor and donor materials.[1,2] The optimal nanoscale phase separation of the donor and acceptor into a bi-continuous network is critical for the performance of plastic solar cell because of short exciton diffusion length (~10 nm) in organic materials. Therefore, the effect of the postproduction treatment on polymer/[6,6]-phenyl-C_{61} butyric acid methyl ester (PCBM) organic solar cells has been studied by several groups.[3-6] However the mechanism behind this effect has yet to be understood clearly. In this report we demonstrate the effects of the postproduction heat treatment on the performance of the bulk heterojunction solar cell based on poly(3-hexylthiophene) (RR-P3HT) and PCBM over a range of different temperatures and durations as well as explore the physical phenomenon behind

the improvement during the treatment. We show the performance of solar cells fabricated on flexible substrates (ITO coated PET) using these optimized heat treatment parameters.

An intrinsic problem associated with organic polymers is their degradation due to oxidation and other factors over time. One way to approach this problem is to encapsulate the device with a transparent, flexible, yet chemically stable material, such as parylene. Our stability study data is now available in reference [6a].

EXPERIMENTAL SECTION

ITO coated glass substrates, <20 Ω/□ with >85% light transmission, were obtained from Thin Film Research. ITO on PET substrates were purchased from Delta Technologies. EL-grade PEDOT-PSS was purchased from Bayer AG, and regio-regular RR-P3HT and PCBM from American Dye Source. All materials were used as received without further purification.

The differential scanning calorimetry (DSC) experiments were conducted on a Perkin-Elmer Pyris Diamond DSC, using typical sample weights of ~7-9 mg. The samples were pressed in a sealed aluminum pan, and the measurements were carried out using a heating and cooling rate of 10 °C/min in an ambient atmosphere.

The absorption spectra were measured on a Perkin-Elmer Lambda 900 UV-VIS-NIR Spectrophotometer.

The current-voltage characteristics were recorded with a Keithley 236 source-measure unit. A calibrated solar simulator (Spectra-Physics) was used as the light source for solar cell efficiency measurements.

We fabricated four devices on each substrate, each having an area of ~9 mm^2. The ITO coated glass substrate was etched and cleaned before being plasma treated for five minutes under O_2 gas. A layer of PEDOT:PSS is then spin coated onto the substrate at 6300 rpm creating a 30-35 nm layer. The sample is then dried by being heated at 110-120°C for 60 minutes in a glove box. The photoactive material is then spin-coated onto the sample at 700 rpm creating a ~50-60 nm layer using a toluene solution consisting of 1:2 ratio of PCBM and RR-P3HT, respectively. The final layer is made up of 65% RR-P3HT and 35% PCBM. An aluminum cathode was then deposited under high vacuum ($>10^{-6}$ torr) at an initial deposition rate of 0.4 Å/s gradually increasing to 1.0 Å/s with a 450 sec ramp time to a final thickness of 1000 Å. A surface profiler (AMBIOS XP-1) was used to measure film thickness. The finalized device is then annealed on a hot plate in a glove box at the desired temperature for the desired amount of time. The flexible devices were created in exactly the same way except for minor modifications in the etching and cleaning process.

Results and Analysis of Post-production heat Treatment

One key contribution of this work was the discovery of effect of molecular weight (MW) for P3HT on the preproduction parameters and the postproduction treatment conditions. Detailed explanations are arranged according to P3HT of different MW used in the device fabrication.

2.1 P3HT with low molecular weight

In this section, P3HT with low MW (20,000 to 25,000 g/mol) was used, which was purchased from American Dye Sources (ADS), Inc.

Figure 2.1.3 Representative DSC thermograms of the regio-regular P3HT sample from ADS (dashed line) and composite of RR-P3HT and PCBM (35 w.%).

Tapping mode atomic force microscopy (AFM, NT-MDT)) topographic imaging was performed on stacks of ITO/PEDOT:PSS/PCBM+RR-P3HT (Figure2.1.4). The surface of the films was smooth. The average profile for each sample is also shown in Fig. 4 below the corresponding AFM images. Rms roughness is 2.17 nm for non-annealed sample but increased to 3.35 nm for the annealed sample at 90 °C for 3 minutes. This indicates improved phase segregation with characteristic dimensions comparable with the exciton diffusion length. As it was shown recently in Ref. [4] by TEM study, the PCBM does diffuse even at temperatures as low as 60°C. At high temperatures PCBM molecules diffuse easily and can form large micron-sized crystals at high PCBM concentrations. Surprisingly, we found that the 3% efficiency of PCBM/RR-RR-P3HT photovoltaic cell can be achieved at rather low concentration of PCBM (35%) in comparison with huge ratio of 1:4 or even 1:5 for MDMO-PPV:PCBM and MEH:PCBM composite film device, respectively.[8,9].

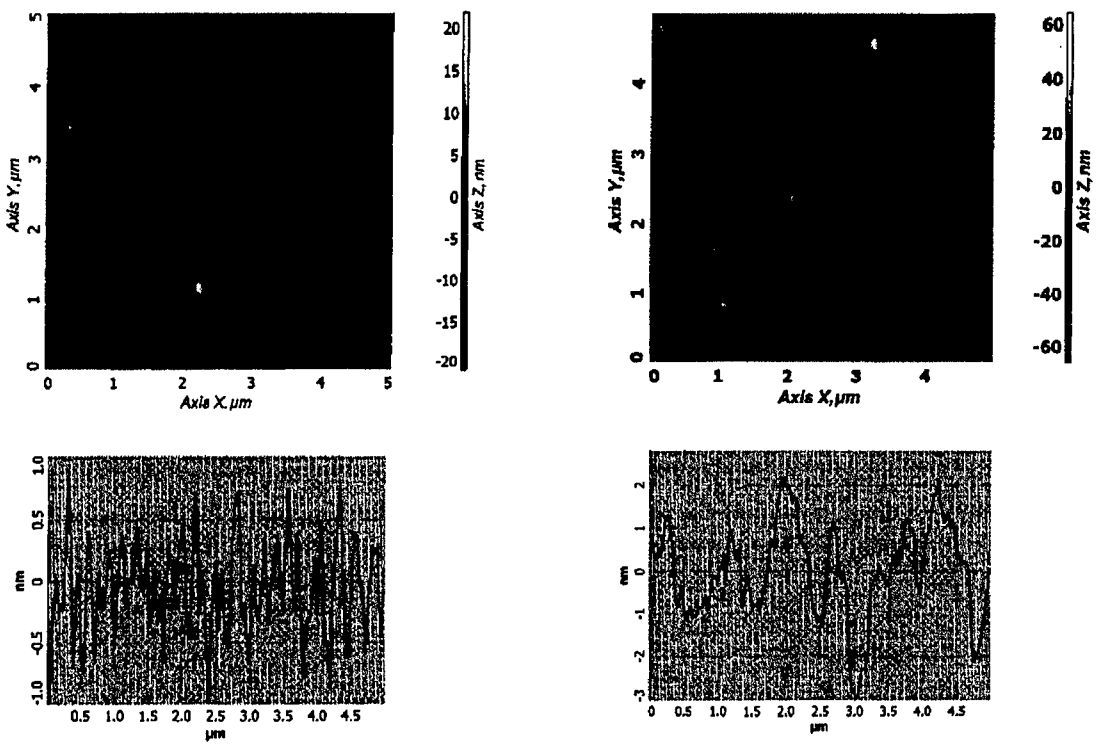

Figure 2.1.4 The 5μm × 5 μm AFM images (tapping mode, amplitude) and average profiles of non-annealed and annealed samples.

The thermal annealing process significantly improves the efficiency of RR-P3HT/PCBM solar cells by improving the morphology of the organic active layer in several ways: 1) densification of the organic film and enhancement of intermolecular interaction which leads to improved absorption of solar light and better electrical transport; 2) optimized phase segregation by enhanced diffusion of methanofullerene molecules in a polymer matrix heated above the glass transition temperature of the polymer; 3) decreased concentration of defects by evaporation of solvent. TEM and selected area electron diffraction study of PCBM/polymer composites has clearly demonstrated the tendency of PCBM molecules to phase separate and form the homogeneously dispersed nanocrystals within polymer matrix.[4] At low concentration PCBM molecules can not form a percolation network within a polymer matrix. At too a high concentration PCBM forms big nanocrystals which are much larger than exciton diffusion length. In this study, we found that optimal concentration of PCBM in RR-P3HT matrix is rather low, only 35 w.%.

An intrinsic problem associated with organic polymers and PCBM is their degradation due to oxidation and other factors over time. One way to approach this problem is to encapsulate the device with a transparent, flexible, yet chemically stable material, such as parylene coating. We have done preliminary experiments and show that it can be done without deteriorating the efficiency of the device.

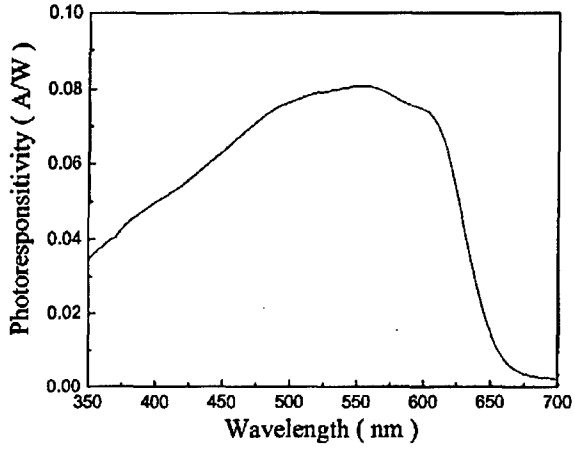

Figure 2.1.5 Photoresponsivity of bulk heterojunction organic solar cell (ITO/PEDOT:PSS/PCBM+RR-P3HT/Al)

Figure 2.1.5 shows the spectral photoresponse of photovoltaic device with glass/ITO/PEDOT:PSS/PCBM+RR-P3HT/Al structure. It is similar to the absorption spectrum.

The rectification ratio increases by an order of magnitude from 10^4 for non-annealed sample to $>10^5$ for annealed one.The best parameters were obtained after annealing at 90 °C for 3 minutes: U_{oc}=0.61V, J_{sc}=14.3 mA/cm^2, FF=0.35 and η=3.05%.

The light intensity dependence of short circuit current density J_{sc} and open-circuit voltage U_{oc} (a), and filling factor (FF) and power conversion efficiency for the typical device (2%) after heat treatment at 90°C for 3 min are shown in Figure 2.1.6. The intensity dependences were measured under white light from solar simulator (Thermoriel) using neutral density filters. The short circuit current density is linearly increasing with intensity indicating negligible bimolecular recombination in the device. FF decreases with increasing intensity. Efficiency reached a maximum 3% at 25 mW/cm^2 and then decreases to 2% at AM1.5 100 mW/cm^2. The reduction in efficiency is due to high serial resistance of the device. The efficiency can be improved significantly (over 20%) by using insertion of thin LiF layer between the organic active layer and the Al electrode and by using low resistance ITO (<10Ω/□). Optimization of the thickness of active layer also needs to be done.

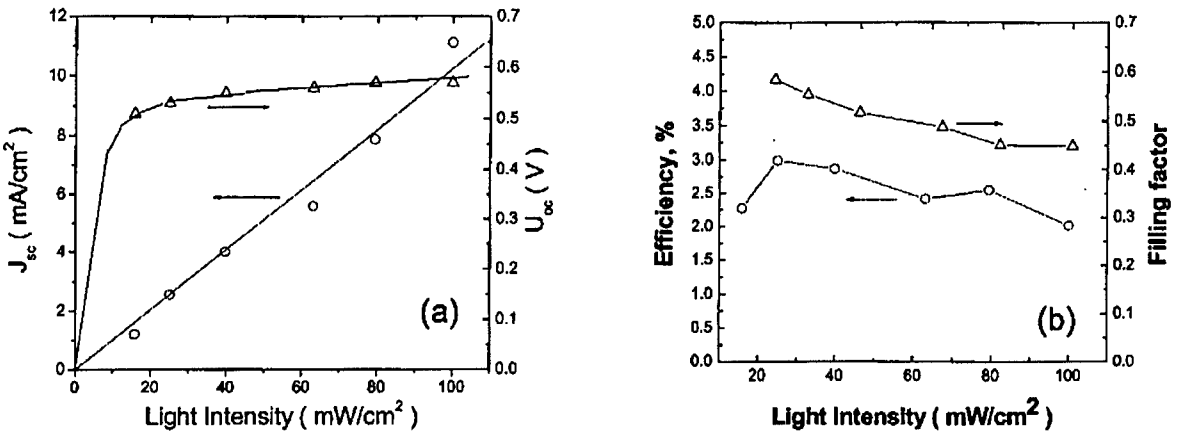

Figure 2.1.6 Short circuit current density and open-circuit voltage (a), and filling factor and power conversion efficiency as a function of the solar light intensity for the device heat treated at 90 °C.

Using the above optimal parameters found with glass ITO substrate devices, flexible solar cell was fabricated on flexible substrates (ITO coated PET, 30 Ω/sq. from Delta Technologies) using the optimized heat treatment parameters; 96°C for 45 sec. We obtained the following parameters for the best device: U_{oc} = 0.59 V, J_{sc} = 9.32 mA/cm^2, FF = 0.49 and η = 2.69%. Figure2.1.7 shows current density-voltage characteristics of such device in dark and under simulated solar light AM 1.5 100 mW/cm^2.

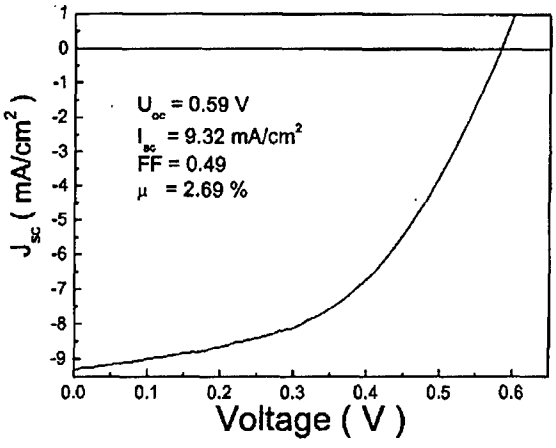

Figure 2.1.7 Current-voltage characteristics of ITO/PEDOT:PSS/PCBM+RR-P3HT/LiF/Al device in dark and under simulated solar light AM 1.5 100 mW/cm^2.

The light intensity dependence of the short circuit current density J_{sc} , the open-circuit voltage U_{oc} (a), the filling factor (FF) and the power conversion efficiency for the typical device after heat treatment at 96°C for 1 min are shown in Figure 2.1.8. The incident light intensity dependences were measured under white light from a solar simulator (Spectra-Physics) using neutral density filters in air. The short circuit current density is linearly increasing with the intensity indicating negligible bimolecular recombination in the device. The FF decreases with increasing intensity. The efficiency reaches a maximum of 2.05% at 25 mW/cm^2 and then decreases to 1.45% at AM1.5 100 mW/cm^2. The reduction in efficiency is due to the high serial resistance of the device.

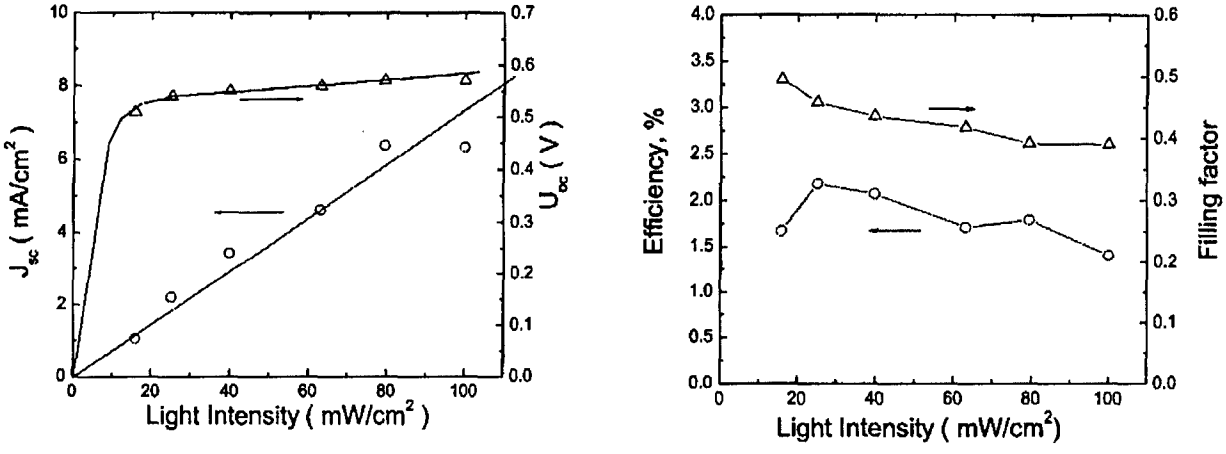

Figure 2.1.8 Short circuit current density and open-circuit voltage (a), and filling factor and power conversion efficiency (b) as a function of the solar light intensity for the device heat-treated at 90 °C.

2.2 P3HT with high molecular weight

Throughout this section, homemade P3HT with a MW of 45,000 g/mol was used. Not only the optimal heat-treatment temperature and duration but also the best PCBM concentration and film thickness were found to be very different from those values found for the devices made with a lower MW polymer. This is due to the different kinetics of diffusion-induced crystallization of P3HT and is associated with the agglomeration of PCBM into a continuous network.

Detailed study [10] have been done with optimalization of the preproduction parameters, (such as concentration of PCBM with respect to the polymer, film thickness and solution concentration) and the postproduction treatment conditions (such as the annealing temperature and duration).

Figure 2.2.1 shows the efficiency depending on PCBM concentration for 8 various temperatures. For each temperature there is a best PCBM concentration and if we connect the best PCBM concentrations for all temperatures, we obtained a linear curve (see figure below). The highest efficiency was observed when the PCBM concentration was around 90% at 155°C and the best PCBM concentration for 200°C (the lowest best efficiency among all temperatures) was determined to be around 82%. For any other temperatures tested during this experiment, the best PCBM concentrations fell between these two values.

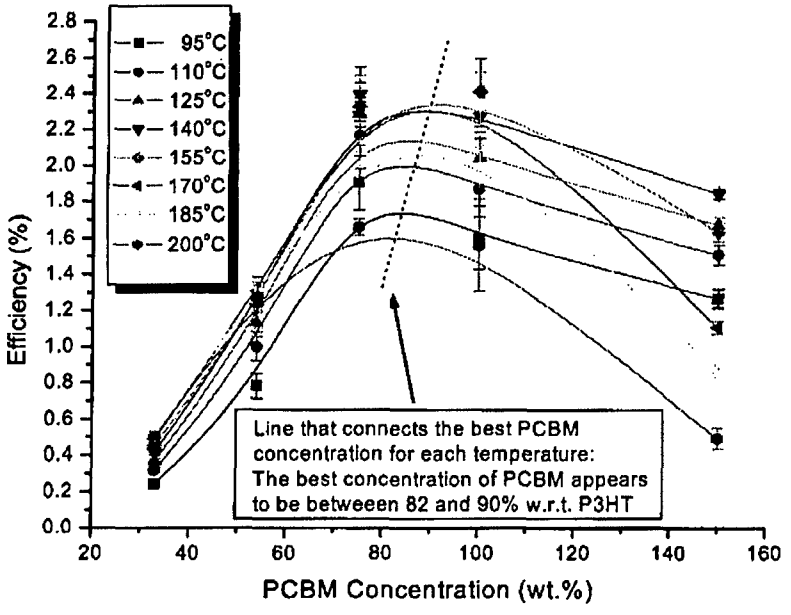

Figure 2.2.1. Efficiency vs. PCBM concentration for 8 different annealing temperatures

Figure 2.2.2 shows the dependence of efficiency via film thickness. The optimal thickness of the film was determined to be around 120 nm, corresponding to a 2.15% solution with 90wt.% PCBM with respect to the polymer. The efficiency increase with respect to the thickness is due to the increase of absorption while the decrease after the optimal thickness can be attributed to the increase of series resistance due to the excessively thick film.

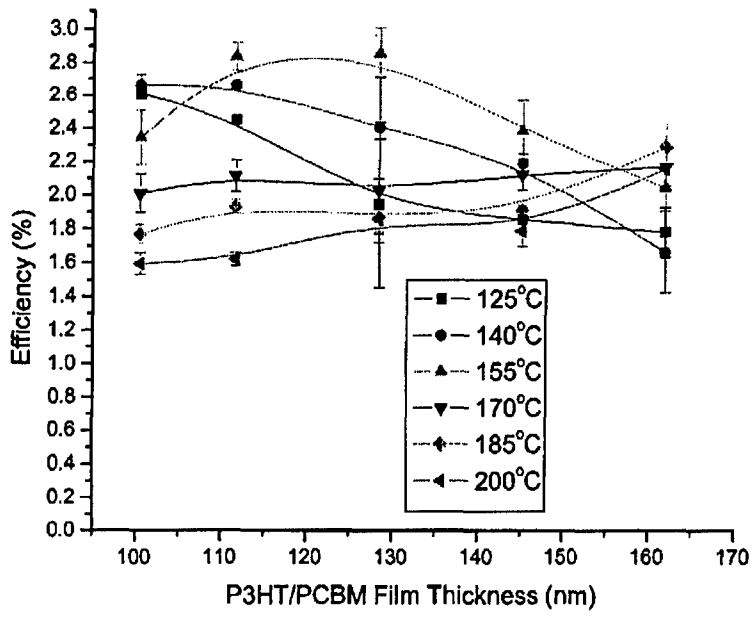

Figure 2.2.2 Efficiency vs. P3HT/PCBM film thickness

Based on the best PCBM concentration and photoactive film thickness found, optimal parameters for the heat-treatment was established. It is clearly seen that the best temperature is 160°C with treatment duration of about 4 min (Figure 2.2.3).

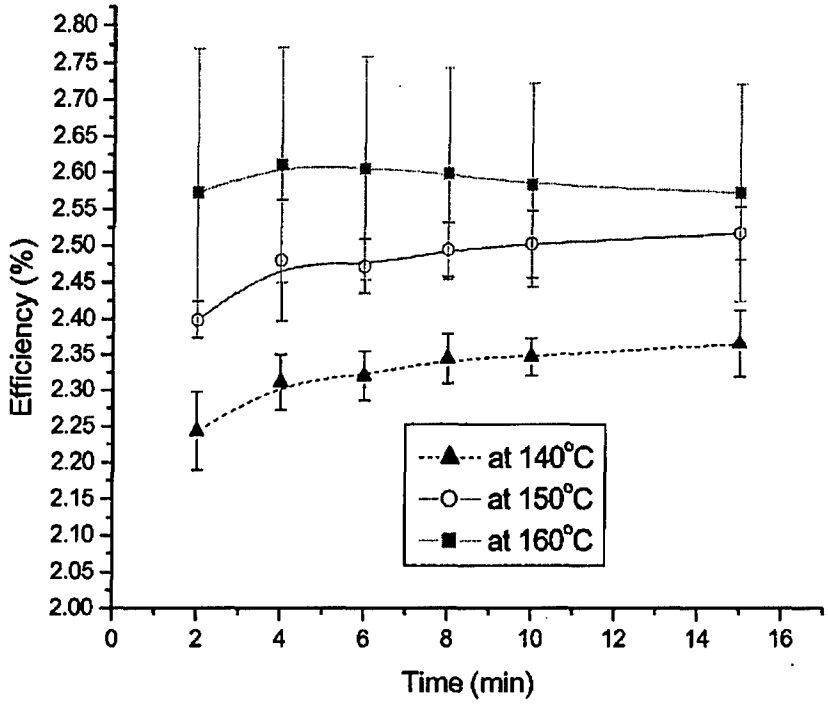

Figure 2.2.3. Efficiency vs. Heat-Treatment Time for three heat-treatment temperatures, the film thickness was 120nm.

Significant differences for the optimal temperature T_{opt} and the duration time t_{opt} were discovered as well as for other optimal pre- and post-production conditions for low- and high-MW P3HT/PCBM composite bulk heterojunction solar cells. It is remarkable that such large differences can be created merely due to employing polymers of different molecular weight. Table 2.2.1 summarizes this work.

Table 2.2.1. Summary of pre- and post-production conditions for high and low MW P3HT/PCBM solar cells

MW	PCBM concentration	Film thickness	Heat-treatment temperature	Heat-treatment duration	V_{oc} (V)	J_{sc} (mA/cm^2)	FF	η (%)
high (45k g/mol)	47%(or 90% wt.%)	120nm	160°C	4min	0.61	8.2	0.65	2.9
low (20k g/mol)	35%(or 54% wt. %)	90nm	97°C	5min	0.61	14	0.35	3.1

2.3 Mixtures of Low and High (or Medium) molecular weight P3HT

In general, higher molecular weight (MW) polymer has higher charge mobility than that of the lower MW polymer in films [11]. This is because the better connectivity of neighboring polymer chains would be expected to make inter-chain transport easier by increasing the electronic overlap between neighboring nano-chains, and longer chains (higher MW polymer) should reduce the number of required inter-chain hops to traverse the film. Upon heat-treatment, the lower MW polymer will easily crystallize and form small crystallites in the film, while the higher MW polymer does not crystallize as readily. It is believed that the charge mobility within crystallites is higher than none-crystallized conjugated polymer; however, the charge mobility increases with the molecular weight thus the length of polymer chain. This is due to the fact that the transport in low-MW films is limited by the boundaries between the crystallites. Long chains in high MW films bridge the ordered regions and soften the boundaries.

Mixing low and high MW polymers takes advantage of both high inter-molecule charge transport through long polymer chains and intra-molecule charge transfer within each crystallite. Long chains provide connectivity between low MW polymer crystallites.

The optimum concentration of high MW polymer with respect to that of low was determined by preparing multiple solutions of different high MW polymer concentrations: 1:0, 9:1, 3:1, 1:1, 1:3, and 0:1. Solo low and high MW polymer solutions mixed PCBM show about 2.5% and 3.0%, respectively. Both 3:1 and 1:3 mixtures showed 20% improvement over solo low MW polymer solution device performance but no improvement over high MW device. However, it is not appropriate to conclude no improvement because the solo low MW polymer devices intrinsically have low charge mobility in the film and in the case of 3:1 mixture mere 20% improvement when mixing with mere 25% of high MW polymer. For the mixture of 1:1 the device performance was improved 70% over solo low MW device and over 40% over high MW polymer device, and for the case of 9:1 mixture the performance was improved over 70% compared to the solo low MW device. These improvements are sign of significant increase of charge mobility in the films. The Figure 2.3.1 shows device performance

versus the high molecular weight polymer concentration with respect to that of low molecular weight polymer, in which two peaks, 9:1 and 1:1, of dramatic performance improvement are shown.

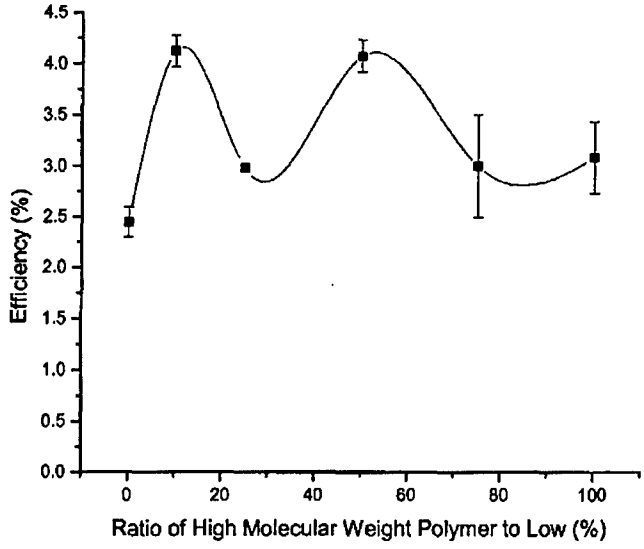

Figure 2.3.1 Efficient versus ratio between high to low molecular weight polymers

Figure 2.3.2 are the IV curves of 9:1 and 1:1 mixtures. The devices show good diode behavior with a high rectification. All four sub-devices in both types performed nearly identical one sub-device to another, indicating that the device fabrication was stable and the results were reliable.

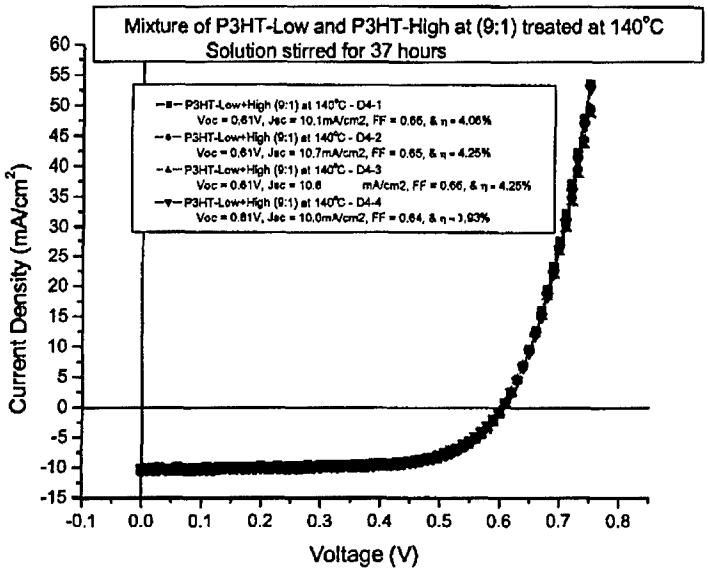

Figure 2.3.2. IV curves of 9:1 and 1:1 mixture devices

In summary high charge mobility was successfully achieved through optimized low and high MW polymer mixtures, resulted in 4.3% power conversion efficiency under AM 1.5 spectrally corrected solar simulator. The optimum mixture of low and high polymers was found to be around 9:1 and 1:1. The two peaks appeared multiple times with a small variation, and are believed to be true results although the physics behind the findings is not clarified yet. A further work needs to be performed to understand the mechanism; however, possible explanations are followings. In case of 9:1 mixture, most of the film consists of low MW polymer nano-crystallites and small portion of longer chains are between the crystallite to help the inter-cluster charge carrier hopping. On the other hand, in case of 1:1 mixture, high MW polymer also forms considerable amount of partial crystallites in the film, and the none-crystallized part of long chains connect crystallites made of low and high MW polymers in the vicinity, resulting in providing high charge mobility.

Part 3. Nanocomposite Solar Cells Based on Conjugated Polymer/ PbSe Quantum Dot

ABSTRACT

We report a novel type of nanocomposite of conjugated polymer (regio-regular polythiophene) with infrared-sensitive, PbSe quantum dots (NC), which have size-tunable lowest-energy absorption bands between 0.3 and 1 e6. Thin film devices show very good diode characteristics and sizable photovoltaic response with an open circuit voltage, *Voc*, of ~ 0.3-0.4 V and short-circuit current density, J_{sc}, of ~ 0.2mA/cm^2, which was significantly higher than recently reported in PbS NC-based devices. This is the evidence of a quite efficient photoinduced charge transfer between the polymer and NC, with infrared sensitivity. Photocurrents under reverse bias are significantly enhanced to $J_{ph} \sim 1$ mA/cm^2, which indicate that the polythiophene/PbSe NC system can be used as effective infrared photodetectors. Quenching of photoluminescence by PbSe NCs has also been studied to gain more understanding of energy and charge transfer in this system. We also investigated the photovoltaic response of similar nanocomposites with poly (2-methoxy-5-(2-ethylhexoxy)-1,4-phenylene vinylene (MEH-PPV). The conduction and valence energy levels of PbSe NCs were determined by cyclic voltametry and reveal type II hetrojunction alignment with respect to energy levels in RR-P3HT for smaller NC sizes. Using these materials, we have observed photovoltaic response at wavelengths as far to the infrared as 2 microns (0.6 eV), which is desirable due to potential benefits of carrier multiplication (or multiexciton generation) from a single junction photovoltaic. Under reverse bias, the devices also exhibit good photodiode responses over the same spectral region.

Introduction

Semiconductor nanocrystals (NCs) have several properties that make them attractive for use as the photoactive material in solar cell. First, the material bandgap can be tuned over a large energy range simply via synthetic control over the NC-size.[12] NCs that have an absorption onset in the near- to mid-infrared (IR) will also strongly absorb solar photons of higher energy. Furthermore, it has been found that NCs efficiently generate multiple excitons upon absorption of single photons of sufficient energy,[13,14] which is a process that has the potential to appreciably increase the photovoltaic power conversion efficiency above the Shockley-Queisser apparent thermodynamic limit.[15] Solution-processable materials such as semiconductor NCs combined with conjugated polymers can promote efficient charge transfer and make possible the production of low-cost, high-efficiency solar cells.

The development of high-quality IR-absorbing NCs[16-19] promises to expand the spectral responsivity of photovoltaic cells to the infrared region of the solar spectrum, which is inaccessible with existing organic materials. Unique challenges are faced in such work, however, since type II heterojunction alignment of the material energy levels becomes difficult for small NC band gaps.,2.e., for large NC sizes. Here we demonstrate photovoltaic performance in PbSe NC-conjugated polymer composites for photon energies as low as 0.6 eV (2 microns).

Here we report studies of both photovoltaic and photodiode response in nanocomposite devices based on PbSe NCs and conjugated polymers. PbSe NCs, which have a bandgap that is size tunable from ~0.3 to 1.5 eV,[16,17] were first studied using cyclic voltammetry (CV) in order to determine the positions of the band edge conduction and valence energy levels. NCs were then combined in solution with either RR-P3HT or MEH-PP6.

Experimental Section

1. PbSe NC synthesis and material preparation

The NCs used in this work were synthesized via chemical routes according to two distinct variations of literature methods [20,21]. After synthesis, NCs were precipitated by addition of methanol, followed by centrifugation. No additional size-selection techniques were employed for either route. All NCs were characterized by PL and absorption spectroscopy, as well as by TEM [20].

A post-synthesis washing was performed to remove the original surfactant by the following steps:
Step 1: blow off excess amount of hexanes by nitrogen gas, until the NCs were barely dissolved;
Step 2: precipitate the NCs by adding 1 ml or more methanol (adding one or two drops of n-butyl alcohol to better precipitate the NCs); remove the solvent along with the now floating surfactant;
Step 3: repeat step 1 and step 2 once more.
Step 4: repeat step 2 two or more times until no visible floating surfactant remained. Then blow-dry using nitrogen gas.

The washed NCs were re-dissolved in chloroform with desired concentration (usually 20 mg/ml). Regio-regular P3HT (RRP3HT) purchased from ADS was dissolved in chloroform with a concentration of 15 mg/ml. Two separate solutions were mixed according to weight ratio 6:1 for NC:polymer.

2. Device Fabrication

ITO coated glass substrates (<15 Ω/sq with ~85% light transmission) were obtained from Delta Technologies, Ltd. EL-grade PEDOT-PSS was purchased from Bayer AG. A 30~35nm layer of PEDOT:PSS was spin coated on a 2.5x2.5cm^2 ITO substrate (with resistance ~40Ω/per □), followed by a heating-dry inside the argon glove box at 100~120 °C for 100 minutes. We fabricated four devices on each substrate, each having an area of ~9 mm^2. The ITO coated glass substrate were etched and cleaned before being plasma- treated for five minutes in O_2 gas.

The photoactive material solution is dispersed by ultrasonication for 10 minutes, followed by heat-up at 60°C for 5 minutes before being spin-coated on ITO substrate at 500 rpm, creating a 100~130 nm layer. An aluminum cathode is then deposited under high vacuum (<10^{-6} torr) at an initial deposition rate of 0.4 Å/s and gradually increasing to 1.0 Å/s with a 450 sec ramp time to create a final thickness of 1000 Å. A surface profiler (AMBIOS XP-1) was used to measure film thickness.

The absorption spectra were measured on a Perkin-Elmer Lambda 900 UV-VIS-NIR Spectrophotometer. The photoluminescence measurements were done on a Perkin-Elmer LS55 spectrofluorimeter. The current-voltage characteristics were recorded with a Keithley 236 source-measure unit. Spectra-Physics solar simulator (150W Xenon lamp with AM0 and AM1.5 filters and focusing lens) with light intensity calibrated at 100 mW/cm^2, was used as the light source for solar cell efficiency measurements. The reported efficiency measurement was not corrected for spectral mismatch.

The IPCE spectrum was taken with a Keithley 236 source-measure unit and a phase-sensitive SR830 lock-in amplifier. The monochromatic light was generated with a monochromator (ThermOriel) coming from a 100W tungsten lamp. The photocurrent was detected by a calibrated Hamamatsu silicon detector for the UV and visible range and a calibrated PbSe infrared detector for the near infrared range.

RESULTS AND DISCUSSION

3.1. Photoluminescence quenching in polymer/NC blend

Figure 3.1.1 shows the linear absorption spectra of three different sizes of PbSe NCs in chloroform solution. It clearly shows the tunability of the band gap (E_g) (from 0.65 to 0.81eV) via size tuning (from 5 nm to 8 nm). It also demonstrates the narrow size distributions. Inset of Figure 1 shows the absorption spectra of thin films of pure RRP3HT and RRP3HT/NC (8nm) blend with the weight ratio of NC over 85%. No appearance of additional peaks indicates there is no or negligible ground state charge-transfer between the polymer and the NCs.

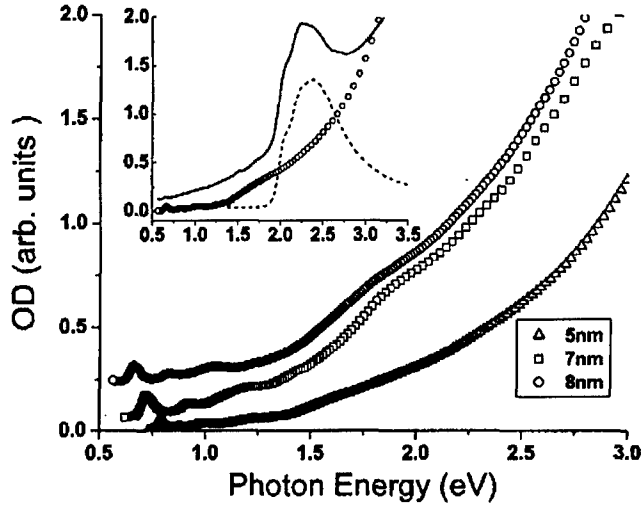

Figure 3.1.1 Absorption spectra of PbSe quantum dots in chloroform solution. Open triangle is for PbSe QDs with average diameter 5nm, open square is for 7 nm and open circle is for 8 nm. Inset shows the absorption spectra of QD 8 nm in solution (open circle), films of pure RRP3HT (dash line) and RRP3HT/QD 8 nm blend (solid line).

PL spectroscopy was applied to further study the interaction between polymer and NC in the excited states. Since regio-regular poly-(3-hexylthiophene) has very small PL, we choose another poly-(3-hexylthiophene), which is regio-random poly-(3-hexylthiophene) (RRaP3HT) to study the PL quenching effect. In Figure 3.1.2 we show the PL intensity as a function of NC concentration by weight (rather than number density). Here two types of NC were used: one is called capped (with the original surfactant layer on), the other is uncapped (washed off the surfactants according to the washing procedure used in the experimental section. There is no significant change of the PL profiles, except that the main peak at 590nm for RRaP3HT PL was constantly shifted to the blue (about 15 nm shift at 80% NC), means the shortening of conjugation length of RRaP3HT due to the introduction of NC.

PL quenching provides evidence for charge transfer between the polymer and the NC, as well as for Förster energy transfer in this case, due to the considerable overlap between PL of RRaP3HT and absorption of NC (Figure 3.1.3). PL quenching is observed even with 10% of capped NC, though very

small, and this effect is increased with NC concentration. PL quenching was mostly due to energy transfer rather than charge transfer in the polymer/capped NC case, due to the in-sufficient quenching of PL even at very high concentration (80%).

With washing-off of the surfactant layer, PL quenching becomes more effective (see dashed lines in Figure 3.1.2), suggesting that charge transfer also took place. As seen from inset of Figure 3.1.3, it is energetically favorable for the electron to hop to the NC from the polymer, creating a charge separation state with the hole remaining on polymer. Even in the case of energy transfer, further separation of charges with hole transferred to the polymer is still possible; again charge separation took place eventually.

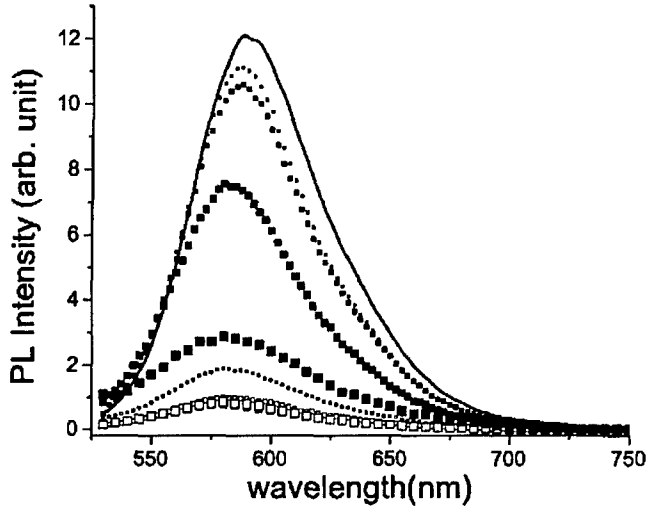

Figure 3.1.2 Photoluminescence quenching of RRaP3HT in nanocomposite film with PbSe quantum dots. The thick solid line is for pure RRaP3HT only, solid squares were for capped (unwashed) PbSe NCs, open squares are for uncapped (4 times washed) PbSe NCs. Size of each symbol corresponds to the weight concentration 10%, 20%, 50% and 80%.

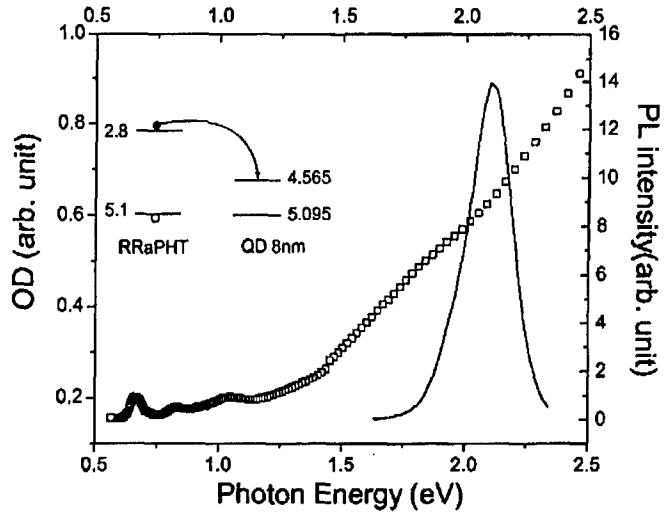

Figure 3.1.3 Absorption of PbSe QD 8nm in chloroform solution and PL of RRaPHT thin film. The solid line represents the PL of RRaPHT, whereas the open square is for absorption of PbSe QD 8nm in solution. The inset shows the energy diagram of RRaPHT and QD 8nm, the values for C-V band were obtained by electrochemical cyclic voltammetry (Figure 3.2.1).

3.2. Nanocomposite solar cells based on conducting polymer /NC blend

In order to construct devices capable of producing a photovoltaic response, we first needed to determine the position of the ionization potential, I_p, and electron affinity, E_a, of PbSe NCs, which to our knowledge has not been reported. CV studies by Sionnest have revealed that both electrons and holes can indeed be injected into PbSe NCs,[22] although use of a pseudoreference electrode prevented energy level assignments. To assign the energy levels, CV was performed on thin films of PbSe NCs, which were drop cast from hexane solution onto a 3-mm diameter platinum working electrode and dried in a vacuum oven at 70°C for 2 hours before loading them into the electrochemical cell. Glassy carbon was used as the counter electrode and the reference electrode was $Ag/AgNO_3$ (0.1M $AgNO_3$ in acetonitrile). All measurements were carried out in a nitrogen-filled dry box to minimize exposure to oxygen and water. Similar CVs were obtained using a gold electrode. The energy levels of PbSe NCs were estimated using NHE potential and a reference ferrocene/ferricinium (Fc/Fc^+) redox couple.[23]

Figure 3.2.1 shows the schematic energy levels of PbSe NCs as well as the levels of MEH-PPV and RR-P3HT (from Refs 24 and 25). It can be seen in Figure 3.2.1 that there is a large energy offset between the conduction bands of the NC and polymer components and there is a much smaller offset between the valence bands. Because the energy levels of the NCs change with size, type II alignment (and thus photovoltaic performance) is expected to be present only for smaller NCs when combined with RR-P3HT. This loss of type II alignment will limit the onset of IR response that is possible with this combination of materials. Furthermore, type II alignment is not expected for any of the NC sizes in combination with MEH-PPV although size dispersion in the NC-component and variation in polymer conjugation length can possibly allow for some photovoltaic response. From the relative

positions of the energy levels, better photovoltaic performance is expected for nanocomposites composed of PbSe NCs and RR-P3HT in comparison to PbSe NCs with MEH-PP6.

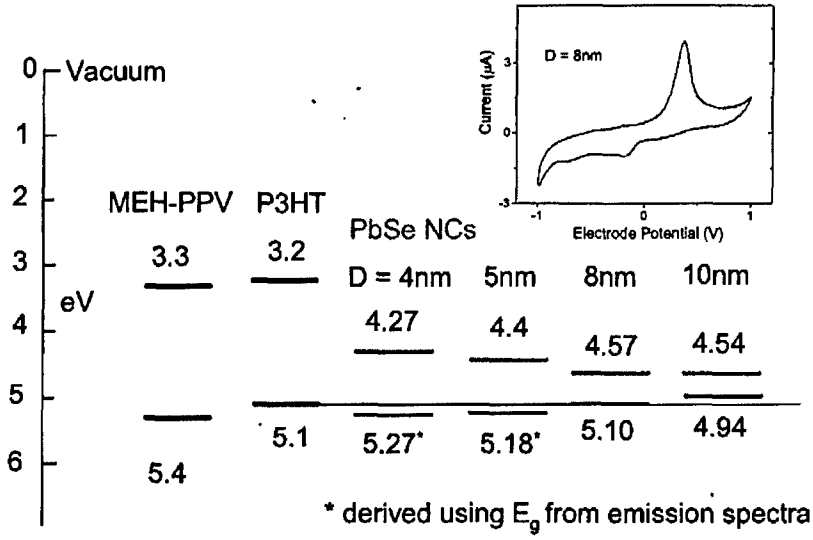

Figure 3.2.1. Energy level positions of MEH-PPV, P3HT, and PbSe NCs of different sizes measured by electrochemical cyclic voltammetry. The dashed line shows the HOMO level of P3HT. Inset shows one example of such cyclic voltammogram recorded at a sweep rate of 20 mV/s for PbSe NCs with diameter 8 nm.

Shown in Figure 3.2.2(b) are the current-voltage characteristics of a device [with the architecture shown in Figure 3.2.2(a)] made with RR-P3HT and 8-nm diameter PbSe NCs. The V_{oc} for this device was 0.34 V, J_{sc} was = 0.2 mA/cm^2, and the power conversion efficiency was 0.04% under AM1.5, 100 mW/cm^2, simulated solar illumination (the efficiency was 0.14% under 10 mW/cm^2 light intensity). Figure 3.2.2(c) shows a comparison of device performance for composites of a fixed NC size (7-nm diameter, bandgap=0.77 eV) when prepared as a nanocomposite with either RR-P3HT (black) or MEH-PPV (red), The weight ratio of NC:polymer was 6:1. It can clearly be seen that the device incorporating RR-P3HT shows significantly better diode characteristics and a larger photoresponse than a similar device consisting of NCs and MEH-PPV, which is consistent with the energy level assignments shown in Figure 3.2.1.

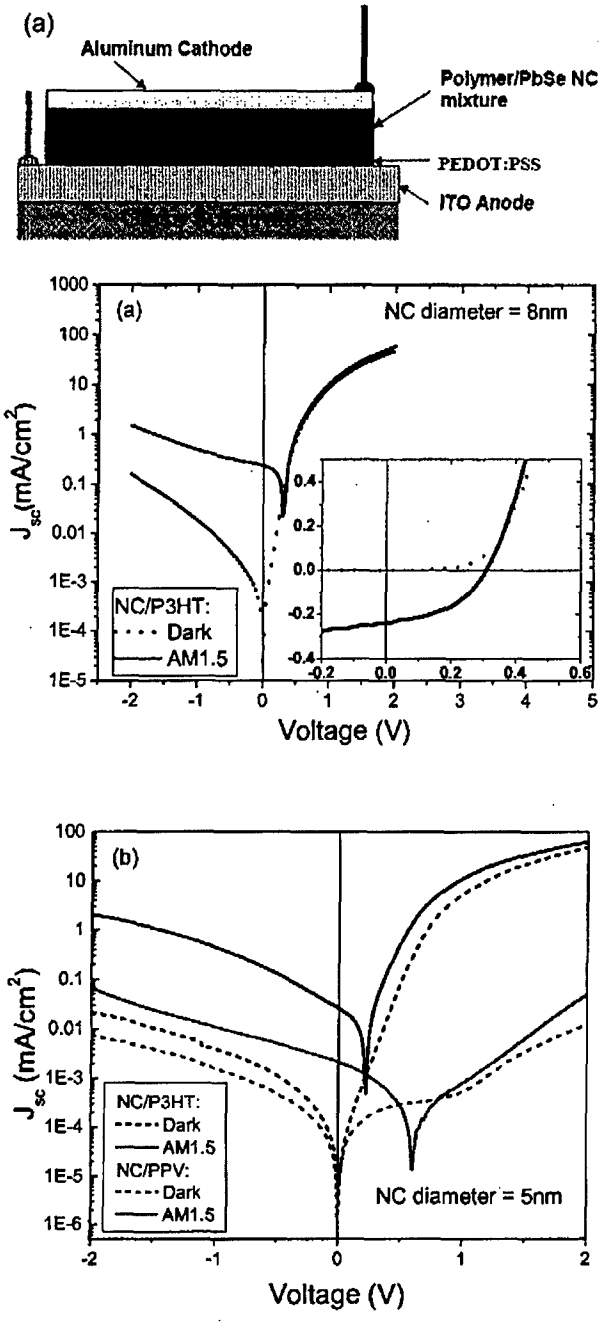

Figure 3.2.2 Comparison of ITO/PEDOT:PSS/Polymer:PbSe NCs/Al (1:6) composites of PbSe NCs with either P3HT or MEH-PP6. (a) Device architecture. (b) Current-voltage characteristics of a device made with P3HT:PbSe NC (E_g = 0.67 eV,8 nm size), with open circuit voltage V_{oc} = 0.32 V, short circuit current density J_{sc}= 0.24 mA/cm^2, fill factor = 0.43 and a power conversion efficiency 0.04%. The inset shows a zoom-in of the region of interest for photovoltaic performance (c) Current-voltage characteristics in the dark (dashed lines) and under AM1.5 illumination (solid lines) for devices made

with P3HT:PbSe NC (E_g = 0.78 eV, 5-nm diameter) (black) and MEH-PPV:PbSe NC (E_g = 0.78 eV, 5-nm diameter) (red).

To investigate the photoresponse originating only from PbSe NCs, we illuminated the devices with a 100-mW, 830-nm cw laser. Figure 3.2.3 shows the dependence of (a) J_{sc} and (b) V_{oc} on NC bandgap. For comparison between various devices, J_{sc} was normalized by the absorption of the composite film at this wavelength. It is clearly shown that the photocurrent has an onset at E_g~0.6 eV (NC diameter = 8 nm), which is also consistent with the energy diagram shown in Figure 1. Upon absorption of the incident photon by NCs, the generated exciton likely dissociates into an electron and hole at the polymer/NC interface. The electron remains on the NC is transported to the Al electrode via hopping between percolated NCs,[30] whereas the hole transfers to the polymer, as long as the type II heterojunction structure is maintained, 2.e., when the NC bandgap is at least 0.6 e6. V_{oc} increases as the NC bandgap increases starting from V_{oc} = 0.15 V for E_g = 0.40 eV (NC diameter = 10nm) and reaches a maximum of V_{oc} = 0.49 V at E_g = 0.81 eV (NC diameter = 5 nm).

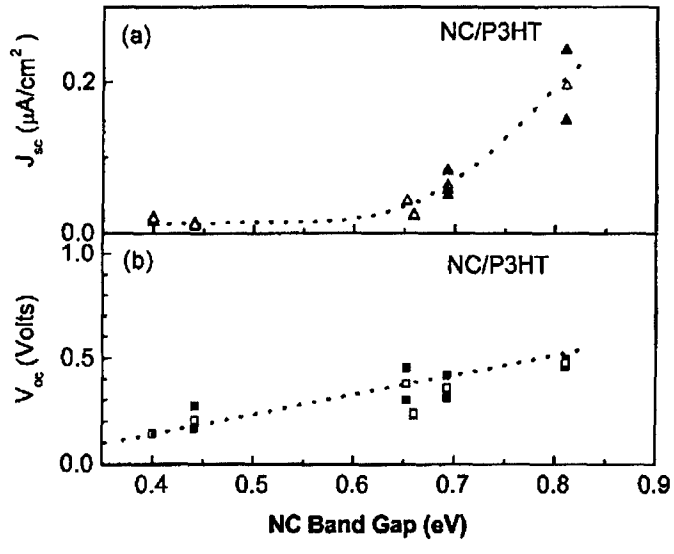

Figure 3.2.3. (a) J_{sc} and (b) V_{oc} dependence on PbSe NC bandgap collected for several devices made from RR-P3HT/PbSe NC devices. Excitation is from an 830-nm CW laser diode with a power of 100 mW. Open triangles and squares represent average values of J_{sc} and V_{oc}, respectively. The dashed line is a guide to the eye.

Figure 3.2.4 shows the incident photon conversion to electron (IPCE) spectrum under photovoltaic conditions (zero bias), as well as the absorption spectra of PbSe NCs for three different NC diameters. Each of the devices shows infrared photocurrent due to exciton formation in the NC followed by charge separation with hole transfer to the polymer. Photoresponse as far to the red as 2 microns is observed.

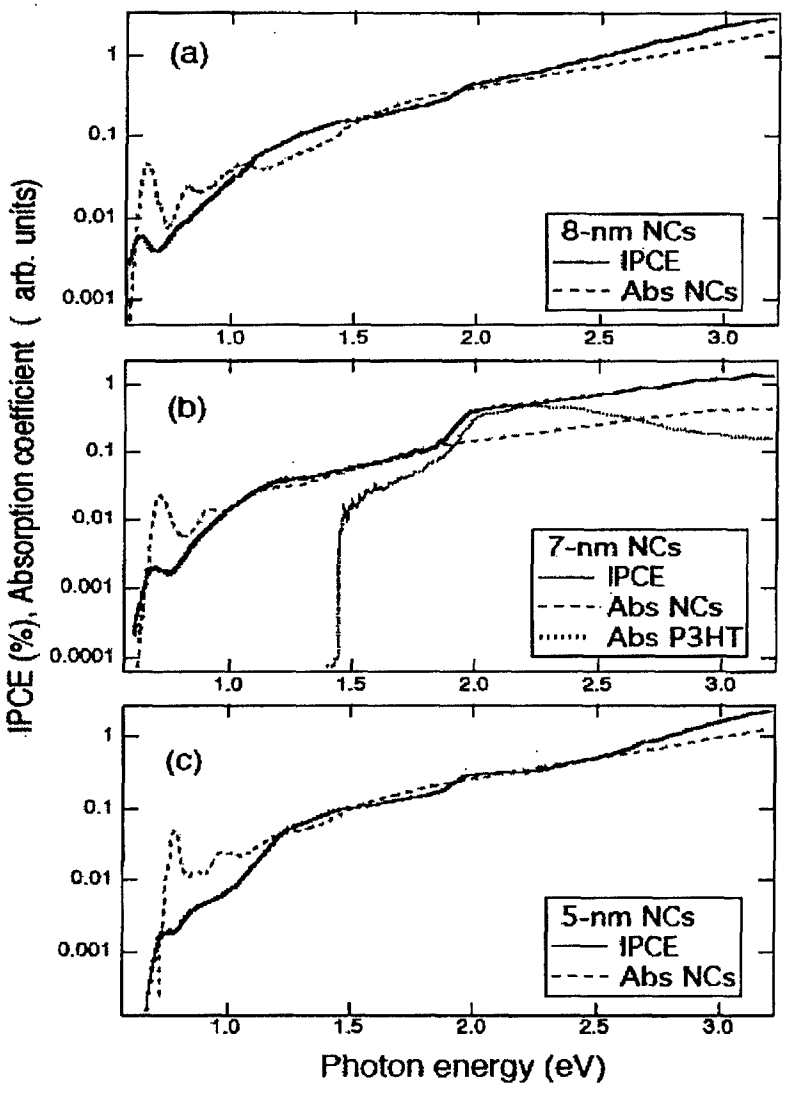

Figure 3.2.4. Comparison between IPCE (solid blue lines) of RR-P3HT/PbSe-NC composite films and PbSe NC absorption spectra (red dashed line) for indicated PbSe NC diameters. The absorption spectrum of RR-P3HT is also shown as a dotted line in (b).

The ICPE and NC absorption spectra roughly correlate over the entire spectral range studied with an IPCE onset that reproduces lowest energy exciton absorption feature of each NC size. These results indicate that the device performance is dominated by light absorption in the NC component of the device. A small contribution from the polymer is manifested as a step at ~2 eV which is most pronounced in Figure 4(b) (in this panel we also show the absorption spectrum of neat RR-P3HT for comparison). While it is known that NCs efficiently produce multiple excitons in response to absorption of a single photon of sufficient energy, it is not yet clear as to if contributions to device

IPCE due to this effect are observed here. The manner in which carrier multiplication is manifested in IPCE measurements depends upon the mechanism for this phenomenon. However, the mechanism of efficient carrier multiplication in NCs has not yet been conclusively determined and, until it is, the only undeniable demonstration of carrier multiplication contributions to photocurrent in a device would be measurement of an IPCE in excess of 100% under zero bias (photovoltaic conditions). It is tempting to compare the IPCE of a device with its absorption spectrum. However, this comparison first requires information about whether or not the carrier multiplication mechanism results in contributions to the oscillator strength of the NC material at wavelengths that produce multiple excitons. Specifically, any mechanism (such as impact ionization) in which a single high-energy exciton is first created that then transfers energy to a valence band electron in the NC that is next excited across the NC energy gap, would not contribute to the absorption spectrum of the NC. In this case, one would expect a deviation (increase) of IPCE relative to the NC absorption spectrum. However, if the process instead occurs via direct photogeneration of multiexcitons, such as in a mechanism that we recently proposed whereby virtual single exciton states facilitate instantaneous production of multiexcitons,[26] these transitions would contribute oscillator strength to the NC absorption spectrum. According to this later mechanism, carrier multiplication would be observed as a *lack* of deviation of IPCE from the absorption spectrum of NCs, which is approximately what is observed in Figure 3.2.4.

The photodiode response of devices consisting of RR-P3HT and PbSe NCs is shown in Figure 3.2.5 for two NC sizes. It can be seen that the application of reverse bias on the devices causes a significant increase in the spectrally-resolved photocurrent with nearly two-orders of magnitude increase of current for low photon energies. The low-energy onset of the photodiode response is also observed to depend upon the NC band gap as in the case of the photovoltaic response.

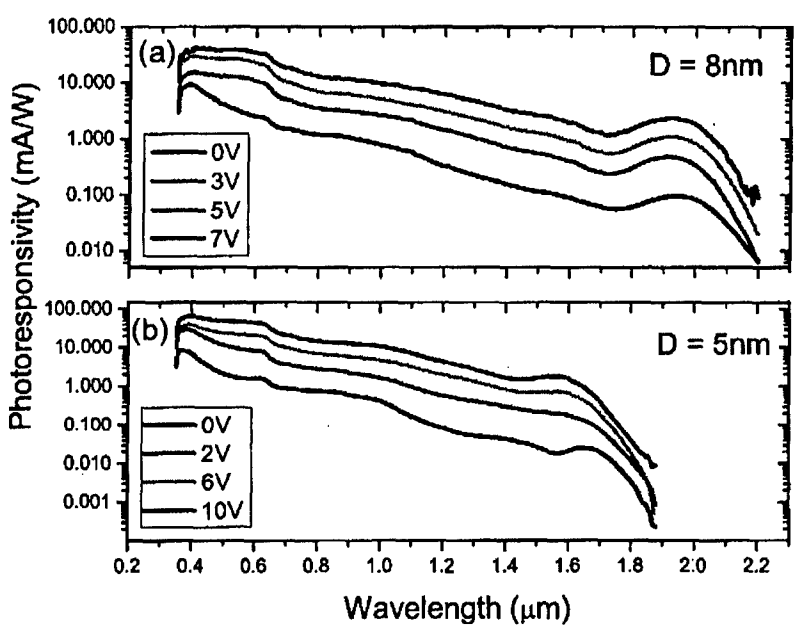

Figure 3.2.5. Comparison of spectral responsivity of RR-P3HT/PbSe-NC devices under applied bias for (a) 8-nm and (b) 5-nm diameter PbSe NCs. The rapid drop of responsivity near 0.38 microns is due to ITO absorption.

In summary, we report studies of nanocomposites of conjugated polymer (RR-P3HT or MEH-PPV) with infrared-sensitive, PbSe NCs. Partial quenching of photoluminescence of RRaPHT by PbSe QDs shown the co-existence of energy and charge transfer in this system. Thin film cells show very good diode characteristics and sizable photovoltaic response with an open circuit voltage, V_{oc}, of ~ 0.3-0.4 V, short circuit currents, J_{sc}, of ~ 0.2 mA/cm^2, and power conversion efficiency 0.04%. Photovoltaic response is observed as far to the red as 2 microns (0.6eV), which is desirable for efficient utilization of both infrared and ultraviolet regions of the solar spectrum. Devices comprised of RR-P3HT show better photovoltaic performance with PbSe NCs, as was expected from novel CV data on PbSe NCs. We argue that it is difficult at this time to make any clear determination regarding observations of carrier multiplication-enhanced photocurrent from spectral analysis due to incomplete understanding of the physical mechanism of the process, as well as transfer of multi charges.

Part 4. Polymeric Solar Cells with Oriented and Strong Transparent Carbon Nanotube Anode

Introduction

Flexible organic photovoltaic cells on elastomeric substrates need a transparent electrode, which is different from traditional ITO. The problem with ITO is that it has poor mechanical properties and is brittle. Creating a substitute for ITO or fluorinated tin oxide (FTO), is one important challenge not only for organic photovoltaics (OPV), but also for dye solar cells (DSC) and many other types of flexible devices.

After the discovery of carbon nanotubes (CNT), it has been realized that carbon nanotubes can be a perfect material for transparent flexible electrodes for optoelectronic devices. [27]

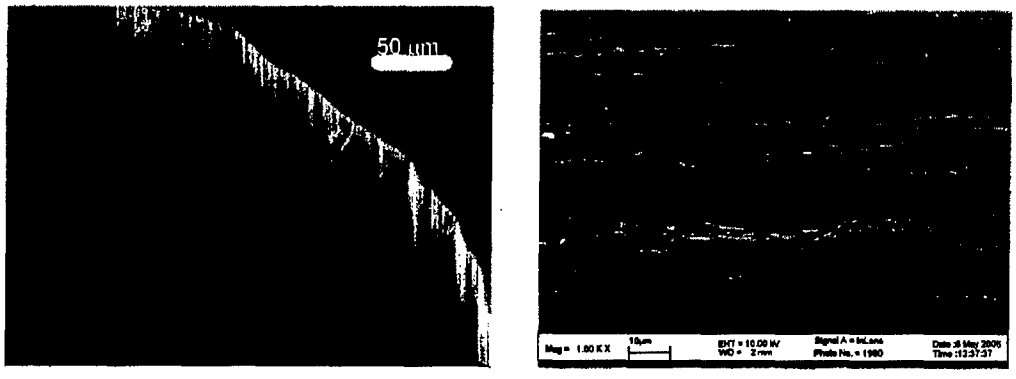

a) b)

Figure 4.1 a) SEM of the CNT sheet being dry drawn from a CNT forrest into a self-assembled sheet. b) Undensified, dry-drawn single layer seet of free standing CNT .

Recently, three groups [28-30] reported on the fabrication and characterization of thin films of carbon nanotubes. All groups have achieved good optical transparency (≥80%) and flexibility, but the transmission was limited to the visible spectral range and the minimum sheet resistance was only ~100 Ohm/sq in the best samples. A.G. Rinzler first noticed high transmittance of a SWNT film in the near infrared (IR) range (3-5 µm). Many transparent conducting coatings (TCC) are transparent in the visible part of the spectrum, but only a few materials retain good transparency in the infrared (IR) while maintaining good electrical conductivity. All three methods are able to produce transparent electrodes, but these electrodes are not strong mechanically, and therefore cannot be in the form of self-supporting, self-sustaining and free standing films, which would be easy to coat without the use of the liquid phase. All three methods used a liquid phase and therefore are strongly limited to use in small area devices.

A new, dry and simple process[27] has been developed which allows one to create CNT-based fibers, yarns, and sheets that are incredibly strong free-standing materials. CNT sheets described herein have exceptional mechanical strength, and can be produced with practically unlimited length and widths of 5-10 cm or more (Figure 4.1).

Carbon nanotube sheets thus self-assembled [27]have the following unique properties and unique property combinations, particularly useful for solar cells: (1) high optical transparency in very broad spectral range from UV to MIR, (2) low electrical sheet resistance, (3) three-dimensional topology of the mesh-like CNT network, which allows charge collection from a large surface area, and not only from a planar interface, like from usual ITO electrodes, (4) extended interface of the three-dimensional network, which enhances charge separation and collection, (5) high thermal conductivities and thermal diffusivities, which provide heat dissipation, (6) high work function required for collection of holes, (7) high flexibility as opposed to brittle ITO and other inorganic TCOs, (8) very high resistance to creep, (9) interpenetrating continuous morphology of the nanofiber network, as opposed to the nonpercollated morphology of nanoparticle electrodes, which is favorable for the collection of charge carriers from bulk heterojunction type architectures, (10) retention of strength even when heated in air at 450°C for one hour, and (11) very high radiation and UV resistance, even when irradiated in air.

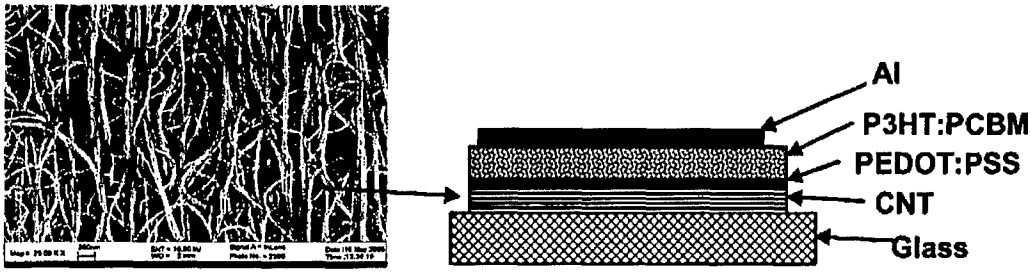

Figure 4.2. Illustration of a solar cell or photodetector based on liquid densified carbon nanotube ribbons as a bottom transparent conducting electrode.

The goal of our work is to create flexible plastic solar cells (SC), using nanoscale composites of conjugated polymers with inorganic components (fullerenes, nanotubes, titania nanofibers) on the load bearing carbon nanotube transparent electrodes in bulk heterojunction solar cell architecture, which we have optimized earlier at ~ 4% efficiency[31]. Figure 4.2 depicts an organic solar cell based on carbon nanotube ribbons as a front-surface transparent conducting electrode, formed on a glass or plastic substrate.

Experimental

A free-standing carbon nanotube (CNT) sheet is drawn laterally from the side of a CNT forest. It is then placed on a clean substrate of Corning 1737 display glass or flexible plastic (PET or PEN). The CNT sheet was densified using surface tension effects of an imbibed liquid (for example, methanol). The rapid evaporation of the solvent absorbed in the sheet causes shrinkage leading to densification. Four devices were fabricated on each substrate, each having an area of ~3 mm^2. A layer of PEDOT:PSS was then spin-coated onto the substrate at 6100 rpm creating a 50-55 nm layer. The sample was then dried by being heated at ~120°C for 45 minutes in a glove box. The photoactive material solution was then spin-coated onto the sample at 700 rpm creating a 175-225 nm layer using a toluene solution consisting of roughly 9:10 weight ratios of PCBM and RR-P3HT, respectively. An aluminum cathode was then deposited under high vacuum (<10^{-6} torr) at an initial deposition rate of 0.4 Å/s and gradually increasing to 1.0 Å/s with a 450 sec ramp time to create a final thickness of 1000 Å. A surface profiler (AMBIOS XP-1) was used to measure film thickness. EL-grade PEDOT-PSS

was purchased from Bayer AG. RR-P3HT and PCBM were purchased from American Dye Source. All materials were used as received without further purification.

The absorption spectra were measured on a Perkin-Elmer Lambda 900 UV-VIS-NIR Spectrophotometer. The current-voltage characteristics were recorded with a Keithley 236 source-measure unit. A solar simulator (ORIEL 300W) with light intensity calibrated at 100 mW/cm^2, was used as the light source for solar cell efficiency measurements. The reported efficiency measurement was not corrected for spectral mismatch. Photovoltaic measurements were done in a nitrogen-filled glove box.

Results and discussion

Bulk heterojunction device architecture of regioregular P3HT and PCBM was created with a CNT anode using extended homogenization by steering followed by heat treatment at the optimal temperature and time .[31] The nanocomposites of home synthesized fresh P3HT with PCBM spin coated on an ITO coted glass substrate at optimal concentration is demonstrated to give a record > 4 % power efficiency. [31] Our AFM studies showed the formation of a fine three-dimensional interpenetrating network.

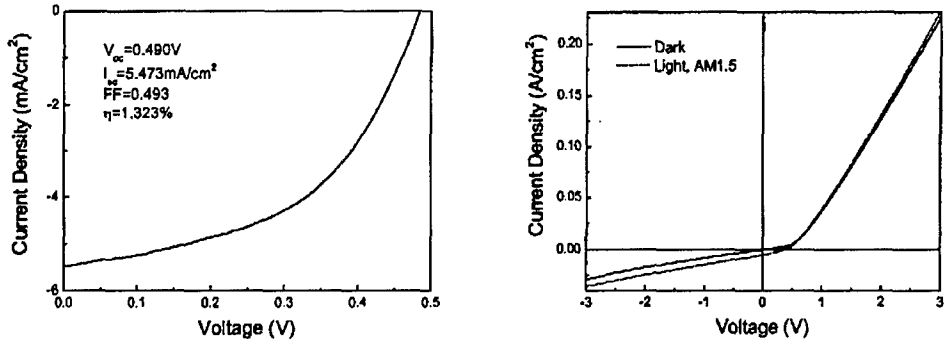

Figure 4.3. Current-voltage characteristics of the best ITO/PEDOT:PSS/PCBM +RR-P3HT/Al device in dark and under simulated solar light AM 1.5 100 mW/cm^2.

For the key task of creating a flexible, mechanical load bearing and transparent charge collection network to substitute for ITO, we have developed several new methods to create multifunctional structures by a simple method of dry spinning self-assembly, as recently described. [27] These structures are based on very thin free-standing sheets of multiwall carbon nanotubes starting from a forest of MWCNTs home-synthesized by CVD.

This method allows one to obtain freestanding, strong ribbons of multiwall CNTs, which are highly oriented, have high optical transparency and can be easily transferred on various flexible substrates or even on ready to use photogeneration layers as effective hole collecting electrodes.

The single CNT sheet has a flat transmission better than 80% over a very broad spectral range from visible (0.4 μm) to infrared (2 μm) (Extended transmission up to 10 μm was shown in ref.27). The resistivity of the CNT sheet parallel to the direction of orientation decreases from 717 Ohm/sq to 605, 603 and 588 Ohm/sq and in the perpendicular direction from 3.96 kOhm/sq to 3.59, 3.54 and 3.47 kOhm/sq with the addition of 1, 2 and 3 layers of PEDOT:PSS respectively. Usually, resistivity of a

carbon nanotube network increases 5-10 times after it is mixed with conducting polymers because of deteriorating intertube contacts. In contrary, spin-coating PEDOT:PSS on top of the carbon nanotube sheet decreases the resistance due to improved densification and, probably, intertube contacts.

Figure 4.3 shows current-voltage characteristics of the best ITO/PEDOT:PSS/PCBM+RR-P3HT/Al device in dark and under simulated solar light AM 1.5 100 mW/cm^2 (Figure 4.3a). Good diode characteristics and, surprisingly high photovoltaic parameters were obtained after annealing at 155 °C for 5 min: an open circuit voltage U_{oc}= 0.49V, a short circuit current J_{sc}= 5.47 mA/cm^2, a fill factor FF = 0.49, and efficiency η = 1.32%.

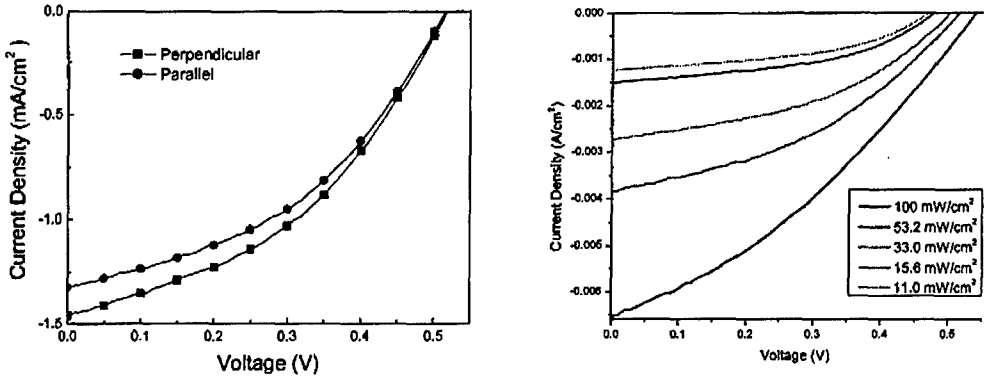

Figure 4.4. a) Current-voltage characteristics of the CNT/PEDOT:PSS/PCBM +RR-P3HT/Al device under simulated solar light AM 1.5 100 mW/cm^2 for two orthogonal polarizations of incident light. b) Dependence of I-V curves on light intensity: filling factor increases at low power, so at 10 mW/cm2 efficiency increases to 2.4 %

The efficiency of our preliminary created OPV SCs with transparent CNT collecting networks is slightly above 1 % at AM 1.5 while at smaller incident photon power of 10 mW/cm2 it increased to 2.4 %, which is significantly higher than earlier reported 0.081% efficiency of MEH-PPV based SCs with non-transparent and thick MWCNT hole collectors. [29] Not only were the previous MWCNTs not mechanically strong structures, but also they were not oriented and transparent.
The CNT sheet electrode shows a polarization effect as seen in Figure 4.4. Current-voltage characteristics of the CNT/PEDOT:PSS/PCBM +RR-P3HT/Al device under simulated solar light AM 1.5 100 mW/cm^2 for two orthogonal polarization of incident light differ by 4.6%. The aligned carbon nanotube sheet can be used in polarization sensitive photodetectors.

In summary, we have demonstrated that an oriented multiwall carbon nanotube sheet can be used as the hole collecting electrode in polymer solar cells with RR-P3HT as the donor material and PCBM as the acceptor material. Relatively high photovoltaic characteristics have been obtained even with a non-optimized carbon nanotube sheet electrode: an open circuit voltage of 0.49V, a short circuit current of 5.47 mA/cm^2. The next major task is creating SWCNT sheets by a method similar to ref. 27. This can be solved since forrests of SWCNT, a precursor for transparent sheets, have recently been grown [32] successfully, and we are now testing suitable forests for making strong sheets.

Part 5. TiO_2 Nanofibers by Electrospinning and Other Methods

We continue to explore methodologies for the fabrication of meoporous TiO_2 fibers. The main approach has been our patent pending electrospinning technique which produces a non-woven mesh of high surface area mesoporous TiO_2 fibers. Application of these fibers in the present solar cell configuration requires nanofibers (<100nm). Ideally the electrospun fibers would have diameters <20nm in diameter. We have been exploring the controlled growth of porous TiO_2 Nanofibers by fine tuning the synthesis variables. There are a variety of parameters that can be adjusted in the electrospinning experiment and we continue to systematically evaluate the effect on nanofiber growth. In parallel, we have examined the controlled etching of e-spun TiO_2 fibers using various acids and bases. While fibers in the 20nm range can be achieved the yield is quite low and may not prove competitive with a direct synthesis method. Another approach to nanofibers is to include polymer spheres (300nm) in the spinning gel that can later be removed thermally or by solvent extraction. It was thought that inverse opal photonic fibers might be generated if the spheres self assembled. The resulting fibers are generally larger than 100nm which may reflect the sphere size, and the arrangement of sphere is random.. Future experiments will involve smaller (<300nm) polymer spheres. Another patent pending approach to electrospun nanofibers involves co-spinning polymers with the TiO_2 molecular sieves. The original strategy involved semiconducting polymers that could be co-spun with the mesoporous TiO_2 in a donor-acceptor arrangement. The TiO_2 fibers in those earlier studies were too large and devices failed as a result. So while we are now examining TiO_2 fibers in the polymer films. The strategy of using a co-spun polymer with the TiO_2 to control size is currently being explored.

Our goal is to exploit the simple method of electrostatic deposition to produce mesoporous TiO_2 fibers. However, we are also examining several hydrothermal techniques for producing fibers or nanorods. The 4 approaches being explored include Dual Templating, Organosilane modified growth, Inverse Opals and Molecular Sieve Templated Growth. The first 2 methods involve using agents that would limit the particle size by interacting with the nucle2. So far these methods have produced nanoparticles but not the high aspect ratio crystals that are desired. The mesoporous inverse opals have proven difficult because the precursor gels are too viscous to penetrate the opal. We are currently preparing clear gels with very low viscosity to overcome this hurdle. One of the more promising approaches is the molecular sieve templated growth of mesoporous TiO_2. In this case a mesoporous silica such as DAMN-1 or SBA-15 is infiltrated with a TiO_2 precursor, generally $TiCl_4$. Upon hydrolysis and removal of the silica, a mesoporous TiO_2 should remain.

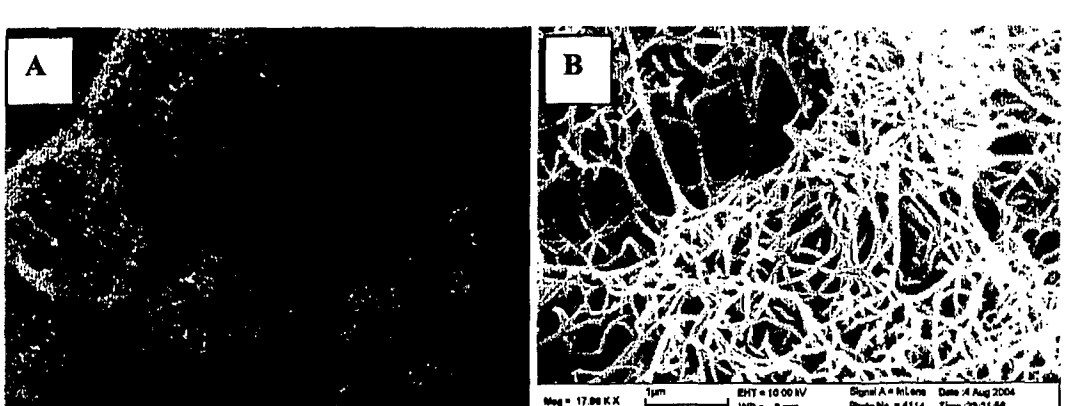

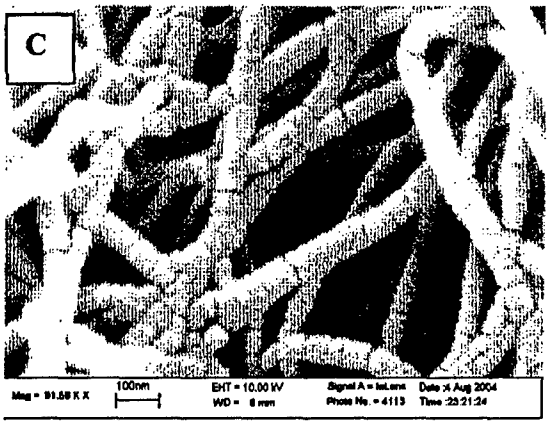

Figure 5.1. SEM images of TiO_2 (anatase) templated from Mesoporous SBA-15.

Figure 5.1A shows the porous TiO_2 Spheres that result from the mesoporous SBA-15 spheres. A closer view in Figures 4.1B and 1C reveal the highly unexpected nanofiber structure. We are currently determining the surface area and pore size of these TiO_2 fibers. However, XRD analysis indicates the nanofibers contain Anatase

In the case of DAM-1 spheres employed as a template even smaller TiO_2 fibers are observed. Figure 10 shows the SEM images of DAM-1 temaplted TiO_2, where again a sphere of nanofibers is formed. Figure 10b reveals the hollow nature of the spheres resulting from DAM-1 removal. The fibers shown in Figure 10c are <20nm in diameter. Again these nanofibers are crystalline Anatase. Interestingly, if the hydrolysis is conducted under an air flow the fibers are predominately Rutile. Normally for mesoporous TiO_2 fibers we do not see a phase transformation from Anatase to Rutile until >800°C. So this reuslt is also unexpected an merits further investigation.

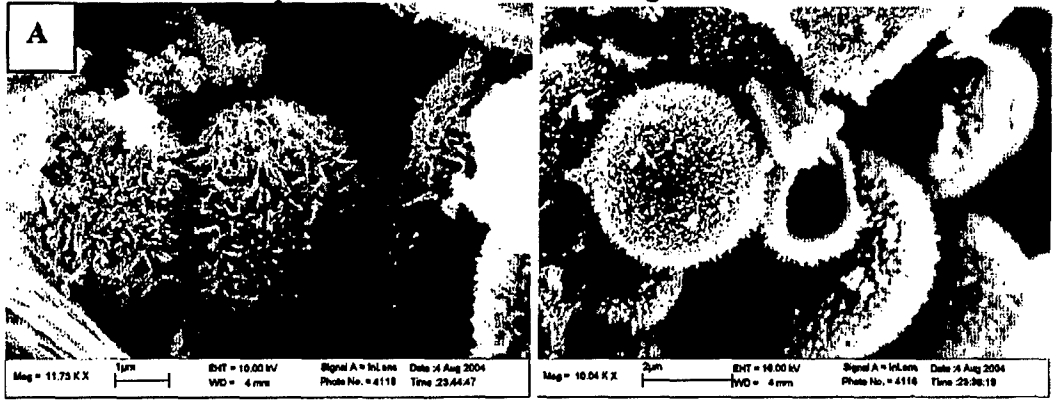

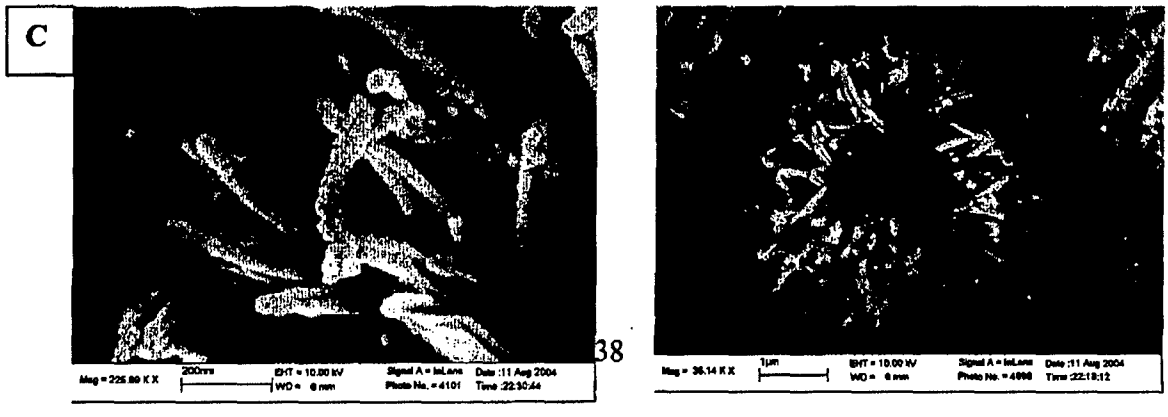

Figure 5.2. SEM images of TiO_2 templated from mesoporous DAM-1 spheres.

Figure 5.2 shows TiO_2 templated by DAM-1 and hydrothermally treated with ammonia. While the titania particle size is as small as in the absence of ammonia, the morphology of the spheres is quite unusual.

One of the advantages of the high surface area and mesoporosity of the TiO_2 nanofibers is the ease at which the pores can be modified. We are currently examining the modification of the mesoporous TiO2 pores with dyes, such as $Ru(bipy)_3^{3+,}$ $Ru(Phen)_3^{3+}$ or metal phthalocyanine complexes. Additionally, we are examing immobilized ionic liquids which could served to up the efficiency as recently reported by Gratzel. We have also explored the formation of carbon nanotube/fiber growth from the TiO_2 to help improve electron transfer.

Part 6. New Polymeric Materials

6.1. Donor-Acceptor block copolymers

We have synthesized several of the polymers (Figure 6.1.1 **7 – 9**) and copolymers first proposed in an effort to control the electronic properties (e.g., absorption, luminescence, ionization potential, electron affinity, etc.) and nanostructures of these components.

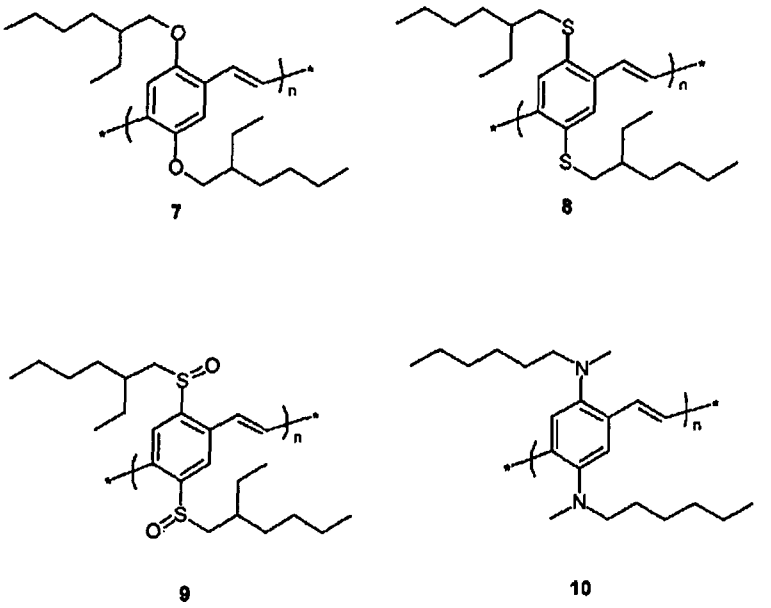

Figure 6.1.1 Examples of modified PPV derivatives. 7 represents BEHM-PPV, 8 for BEHSO-PPV, 9 for BEH-PPV and 10 for BAM-PP6.

The remarkable effect of the heteroatom substitution can be seen from the photoluminescence of polymers **7 – 9**, which tracks with the electron-withdrawing strengths of the substituents (S=O > S > O), as shown in Figure 6.1.2.

Figure 6.1.2. BEHSO-PPV, BEHM-PPV, and BEH-PPV: Polymer films under UV light

Figures 6.1.3 shows the synthetic scheme followed to prepare a novel S-containing monomer. Once polymerized using our patented (US 6,426,399) and patent-pending techniques, a new S-containing conjugated polymer, BEHM-PPV (**7** in Figure 5.1.1) was obtained. Oxidation of **7** afforded polymer BEHSO-PPV (**8** in Figure 5.1.1). These two systems and the previously synthesized BEH-PPV (**9** in Figure 5.1.1) provide a series of structurally related PPV derivatives that range from moderate donor (BEH-PPV) to acceptor (BEHSO-PPV).

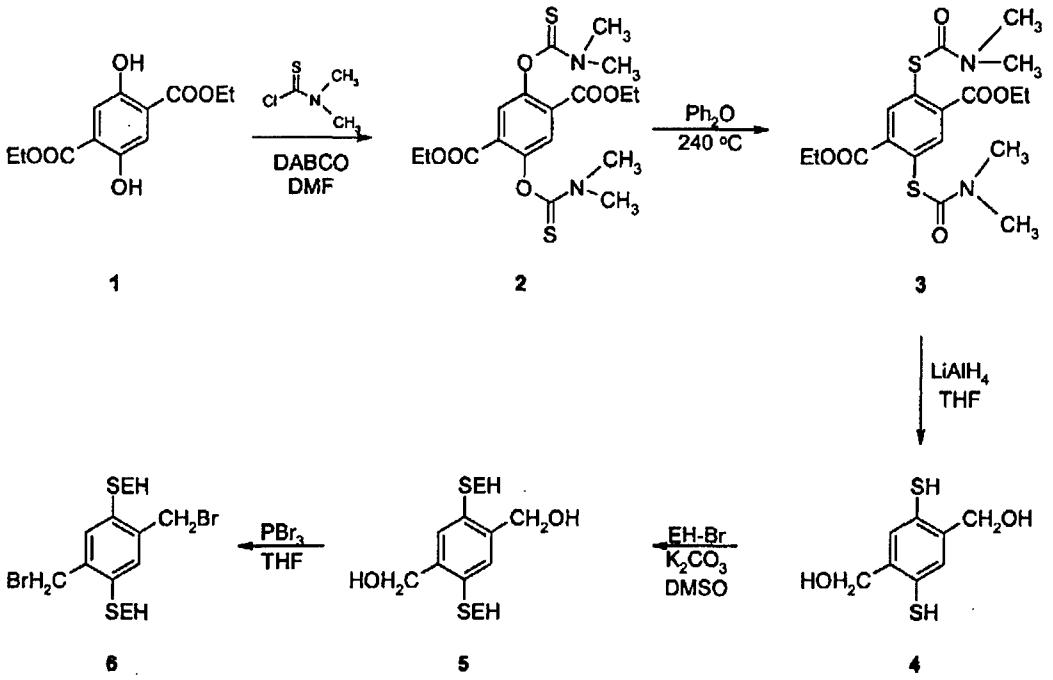

Figure 6.1.3. Synthetic scheme for BEHM-PPV monomer (**6**), obtained in 65% overall yield from **1**.

With the addition of the excellent donor polymer, BAM-PPV (**10** in Figure 6.1.1), also prepared using our polymerization technique, we now have the building blocks to construct Donor-Acceptor *block copolymers* that are anticipated to microphase separate at dimensions comparable to the exciton diffusion length. An AFM micrograph of a block copolymer prepared using related PPV derivatives is shown in Figure.6.1.4.

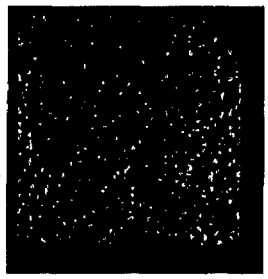

Figure 6.1.4: Tapping mode AFM (5 μm x 5 μm) of *block copolymer* of two substituted PPV derivatives (MEH-PPV and DMOS-PPV)

6.2. Functionalized Poly-3-hexylthiophene Derivatives

In this project we propose instead of mixing two components (infrared PbSe/PbS nanocrystals and P3HT) by stirring, which normally resulted in either severe aggregation of NCs (when the NCs were washed to get rid of surfactants), or very weak charge transfer between the two components). Moreover, there are significant challenges associated with the use of standard ligand-exchange techniques such as surface oxidation, changes in quantum dot size and size distribution and hindered charge transfer processes.

The goal of the proposed research is to develop new synthetic methods enabling the effective attachment to PbSe (PbS) nanocrystals the chains of conjugated polymers, especially polythiophenes (PTs), as well as to understand the chemistry of the nanocrystal-polymer interface. Currently we are exploring the so-called

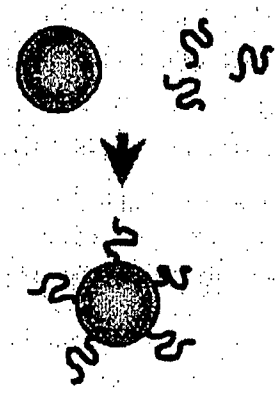

Figure 6.2.1. Grafting onto approach. Semiconducting nanocrystals and polymeric chains are prepared separately. Chemical functionalities are introduced during synthesis of each component. This function-alities are used later to couple polymer chains to the nanocrystals surface.

Grafting onto approach (Figure 6.2.1). It is not very clear if selecting the appropriate nanocrystal and conducting polymer in the premises of weak interaction between them could achieve good results. But it would be interesting to study the charge separation process if interaction between nanocrystal and conducting polymer is enhanced, not only when the respective aggregates be downscaled, but also distance between them can be varied. One way to achieve this is to chemically modify conducting polymers to bear some functional groups such as amino, thiol, phosphine oxide and carboxylic group, which are capable of incorporating with nanocrystals. The advantages of this approach are ability to obtain well-defined core size and ligand length and simple characterization due to separate access to both components.

Conducting polymers that was used in this study is polythiophenes (PTs) (Figure 6.2.2) and we will further extend the study for PPVs, for which there are so far no literature reported efforts to prepare PPVs that bear the functional group on the end of their polymer chain, or on the end of their side chain. For PTs, previous reports have shown ability to control the end of its polymer chain (amino group terminated polyalkylthiophene[35]) and the end of its side chain.[36] We prepared PTs with different functional groups to study their interaction with nanocrystals. Figure 6.2.2 shows the synthetic Scheme of functionalized Poly-3-hexylthiophene Derivatives with different functional groups. Unfortunately the modified PHT from synthesis route 1) and 2) were insoluble in most organic solvents.

1) Synthesis of 2,5-dibromo-3-hexylthiophene using method in ref 33

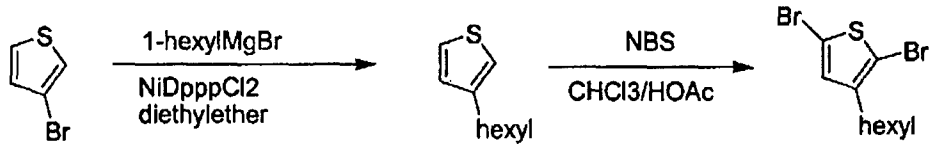

2) Synthesis of 2,5-dibromo-3-(6-bromohexyl)thiophene using method in ref 34

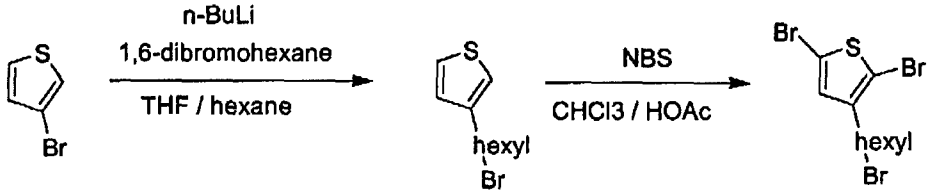

3) Synthesis of Poly-3-(6-aminohexyl)thiophene using method in ref 34 with modification

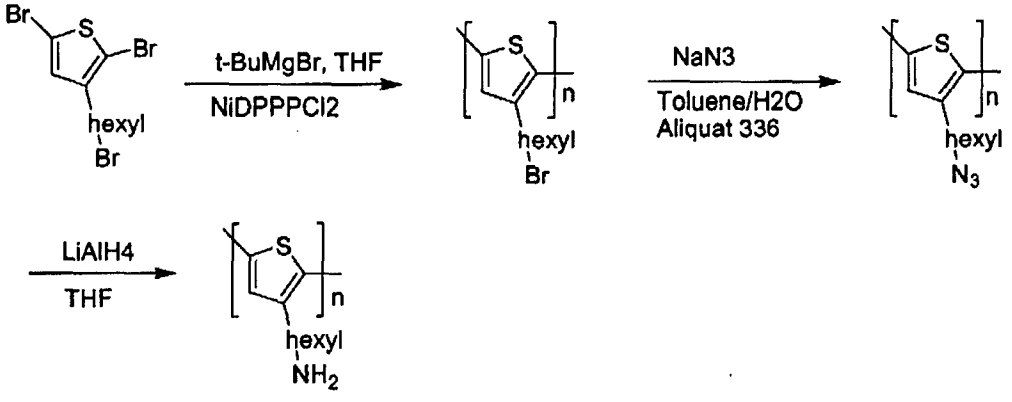

4) Synthesis of Poly-3-hexylthiophene-co-Poly-3-(6-diethylphosphineoxido-hexyl) thiophene

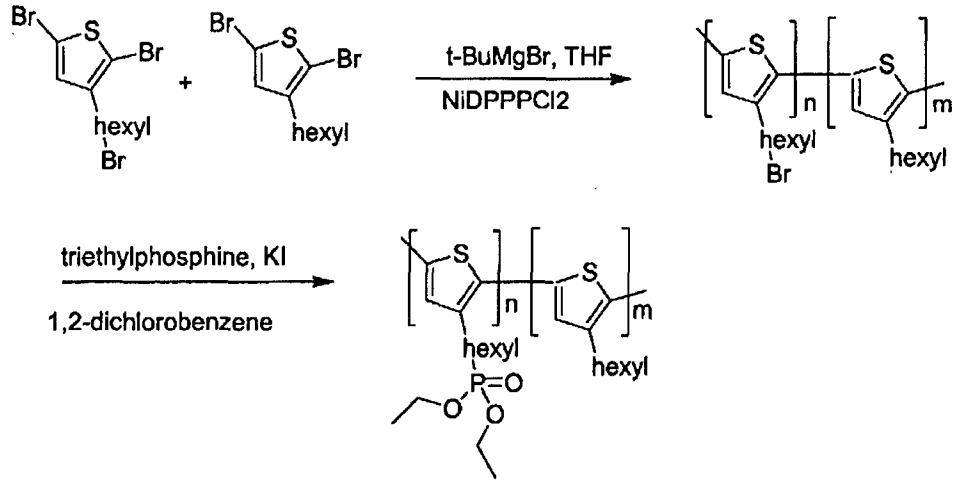

Figure 6.2.2. Synthetic Scheme of functionalized Poly-3-hexylthiophene Derivatives with different functional groups: 1) for dibromo, 2) for dibromo-(6-bromohexyl), 3) for hexylamine and 4) for TOPO.

Characterizations have been done with functionalized PHT according to synthesis route 3). Figure 5.2.3 shows the absorption spectrum measured by FTIR spectrometer. It clearly shows the successful substitute of hexylamine side chain, which can be seen from the good match of PHT-hexylamine and the pure hexylamine.

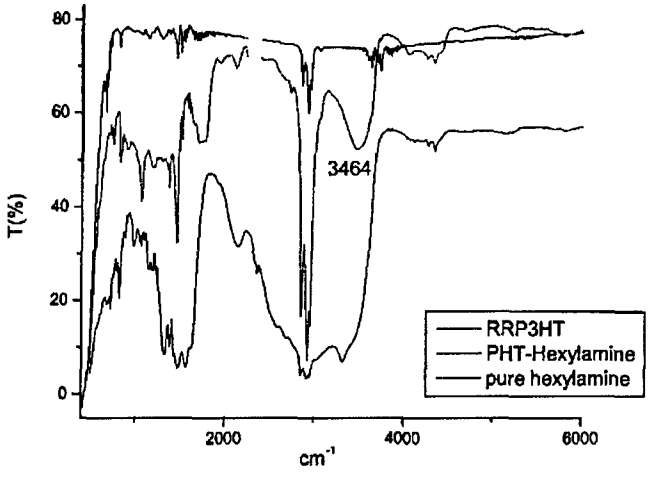

Figure 6.2.3. FTIR spectra for pure RRP3HT (black), PHT-hexylamine (red) and hexylamine (blue). N-H stretching mode was shown at a frequency of 3464cm^{-1}.

Figure 6.2.4 showed the absorption (a) and photoluminescence (b) spectrum of PHT-hexylamine compared with region-regular PHT and region random PHT. It could be seen that the baddgap of this modified PT lies between RRP3Ht and RRaPHT, the considerably bigger PL intensity than that of RRP3HT indicated that the planarity of this modified polymer was not as good as RRP3HT, where the

formation of 2D-lamminae was observed [37,38] before, which accounts for the much better transport properties of RRP3HT as compared with other conducting polymers. The addition of Hexylamine to the side hexyl chain probably made the modified polymer more susceptible to twisting and coiling, which eventually impaired the rigidity and plannarity of the PT backbone.

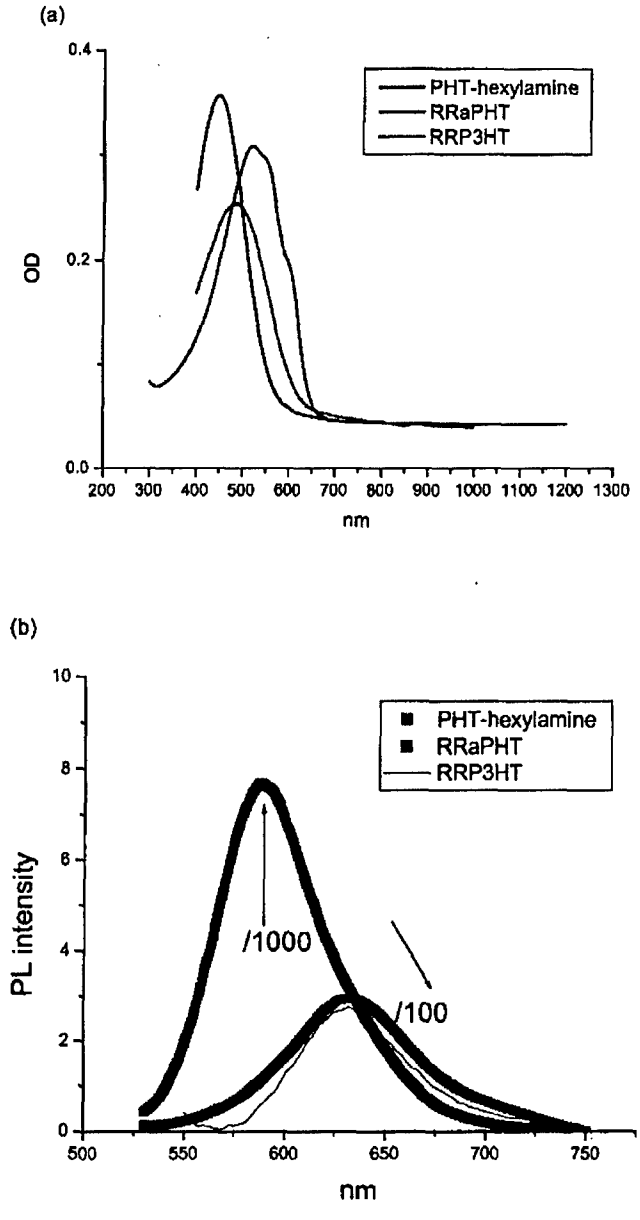

Figure 6.2.4 Absorption (a) and photoluminescence spectra of the modified PHT-hexylamine as compared with RRP3HT (blue) and RRaPHT (black).

Figure 6.2.5 shows the AFM images of two composite films (a) PbSe/RRP3HT and (b) PbSe / PHT-hexylamine, with the weight ratio 6:1 between NC and polymer in both cases. It clearly showed that the one with PHT-hexylamine has better dispersion of NCs within the matrix of polymer, in terms of smaller aggregation of NC and more NCs visible on the surface.

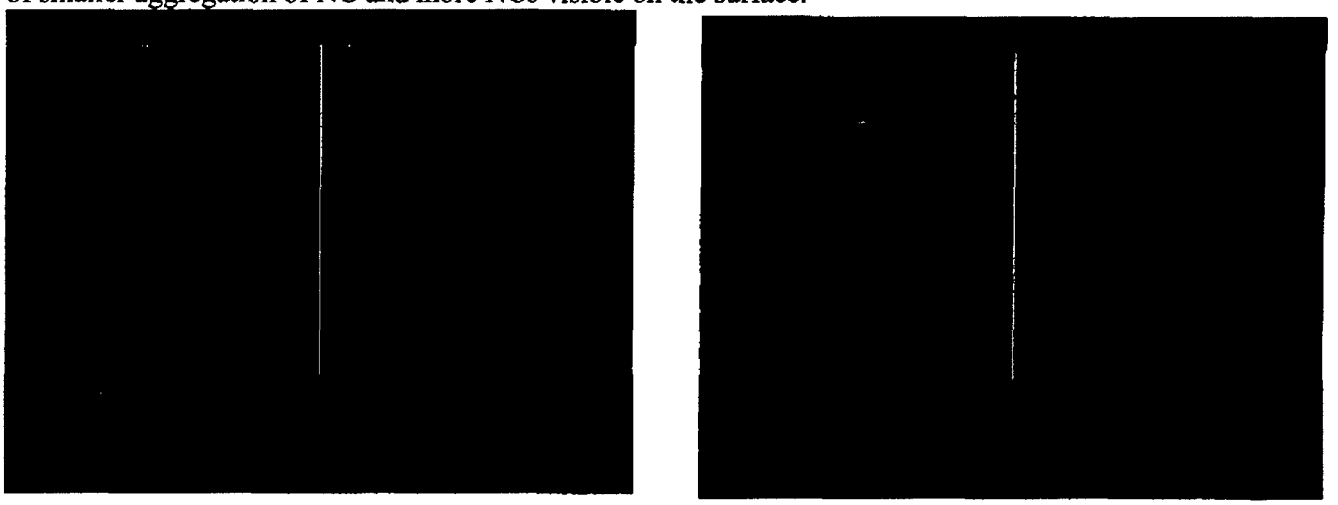

Figure 6.2.5. AFM images of two composite films: (a) PbSe with RRP3HT;(b) PbSe with PHT-hexylamine.

Figure 6.2.6 was the in-plane XRD spectrum of two polymer films, both showed good crystalline structure.

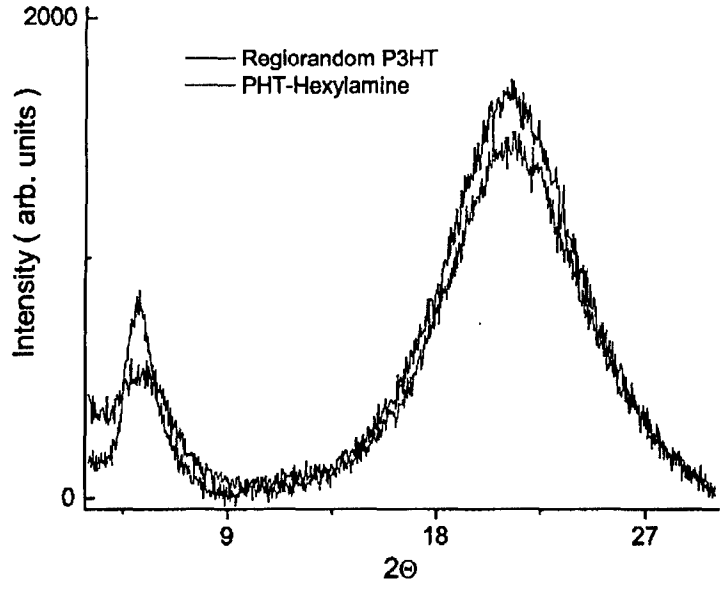

Figure 6.2.6. XRD spectrum of two polymer films: (a) RRP3HT (blue) and PHT-hexylamine (red)

We are currently working on testing the hybrid solar cells made with the nanocomposite of PbS and the new polymer. Efforts have been put to optimize performance of these cells, based on the parameters found with the PbSe/RRP3HT composite solar cells described in part II of this report.

CONCLUSION

In summary, we presented the detailed study of postproduction heat treatment of organic solar cells based on RR-P3HT:PCBM composite in a wide temperature range from 75 °C to 150 °C. The efficiency of the photovoltaic device was significantly improved by postproduction heat treatment and both optimal annealing temperature and time dependencies were determined. The optimal phase separation of PCBM and RR-P3HT into bi-continuous network structure occurs within very short period of time and is very stable. We found that the optimal concentration of PCBM in RR-P3HT matrix is rather low, only 34 w.%. We have also found that the best solvent for formation of optimal interpenetrating network in PCBM:RR-P3HT composite film is toluene. We conclude that the bulk heterojunction photovoltaic device based on PCBM/RR-P3HT composite film is very promising for practical applications.

We also report studies of nanocomposites of conjugated polymer (RR-P3HT or MEH-PPV) with infrared-sensitive, PbSe NCs. Thin film cells show very good diode characteristics and sizable photovoltaic response with an open circuit voltage, V_{oc}, of ~ 0.3-0.4 V, short circuit currents, J_{sc}, of ~ 0.2 mA/cm^2, and power conversion efficiency 0.04%. Photovoltaic response is observed as far to the red as 2 microns (0.6eV), which is desirable for efficient utilization of both infrared and ultraviolet regions of the solar spectrum. Devices comprised of RR-P3HT show better photovoltaic performance with PbSe NCs, as was expected from novel CV data on PbSe NCs. We argue that it is difficult at this time to make any clear determination regarding observations of carrier multiplication-enhanced photocurrent from spectral analysis due to incomplete understanding of the physical mechanism of the process, as well as transfer of multi charges.

We have demonstrated that an oriented multiwall carbon nanotube sheet can be used as the hole collecting electrode in polymer solar cells with RR-P3HT as the donor material and PCBM as the acceptor material. Relatively high photovoltaic characteristics have been obtained even with a non-optimized carbon nanotube sheet electrode: an open circuit voltage of 0.49V, a short circuit current of 5.47 mA/cm^2. The next major task is creating SWCNT sheets by a similar method. This can be solved since forrests of SWCNT, a precursor for transparent sheets, have recently been grown successfully, and we are now testing suitable forests for making strong sheets.

The TiO_2 nanofibers are produced by different methods, but incorporation of them into solar cells architecture still remains a major problem. We are now exploring methods to make them shorter by ultrozonication cutting.

Unfortunately due to low density morphology, with very "spongy" structure of nanofibers, It was not possible to incorporate yet TiO_2 components into solar cells.
While the work is going on improving the morphology, we have started a new route for inorganic component of our hybrid solar cells, by testing nanocrystals of very small size (7-10 nm) of PbSe and PbS, purchased from Evident Technologies. A post doc, Dr. Xiaomei Jiang, was hired for our internal SPRING program, who helped in present AFOSR program to develop this new route.

Novel polymers are synthesized, including Donor/Acceptor block copolymers and functionalized PHT. Their optical and electric properties were characterized, and we started testing their application in both photovoltaic cells and photodetectors.

ACKNOWLEDGMENTS

The authors thank the Air Force Office of Scientific Research for the financial support of this work (F49620-03-1-164), and SPRING Consortium of Texas (Strategic Partnership for Research in Nanotechnology) for the support of the AFOSR program by a new quantum dot and carbon nanotube hybrids approach..

REFERENCES

[1] Yu, G.; Gao, J.; Hummelen, J. C.; Wudl, F.; Heeger, A. J. "Polymer Photovoltaic Cells: Enhanced Efficiencies via a Network of Internal Donor-Acceptor Heterojunctions", *Science* **270,** 1789-91 (1995).

[2] Halls, J.J.M.; Walsh, C.A.; Greenham, N.C.; Marseglia, E.A.; Friend, R.H.; Moratti, S.C.; Holmes, A.B. "Efficient photodiodes from interpenetrating polymer networks", *Nature* **376,** 498-501 (1995).

[3] F. Padinger, R.S. Rittberger, N.S. Sariciftci, "Effects of Postproduction Treatment on Plastic Solar Cells", Adv. Funct. Mater. **13,** 85-88 (2003).

[4] X. Yang, J.J.K. van Duren, R.A.J. Janssen, M.A.J. Michels, J. Loos, "Morphology and Thermal Stability of the Active Layer in Poly(*p*-phenylenevinylene)/Methanofullerene Plastic Photovoltaic Devices", *Macromolecules* **37,** 2151-58 (2004).

[5] J.J.K. van Duren J. Loos, F. Morrissey, C.M. Leewis, K.P.H. Kivits, L.J. van IJzendoorn, M.T. Rispens, J.C. Hummelen, R.A.J. Janssen, "In-Situ Compositional and Structural Analysis of Plastic Solar Cells, *Adv. Funct. Mater.* **12,** 665-9 (2002).

[6] N. Camaioni, G. Ridolfi, G. Casalbore-Miceli, G. Possamai, M. Maggini "The Effect of a Mild Thermal Treatment on the Performance of Poly(3-alkylthiophene)/Fullerene Solar Cells", *Adv. Mater.* **14,** 1735-38 (2002).

[6a] P. Madakasira, K. Inoue, R. Ulbricht, S.Lee, M. Zhou, J.P. Ferraris and A.A. Zakhidov, "Multilayer encapsulation of plastic photovoltaic devices", *Synth. Met.,* **155**(2), 332-335,2005.

[7] P.J. Brown, D.S. Thomas, A. Köhler, J.S. Wilson, J.-S. Kim, C.M. Ramsdale, H. Sirringhaus, R.H. Friend "Effect of interchain interactions on the absorption and emission of poly(3-hexylthiophene) " *Phys. Rev. B* **67,** 0642031-16 (2003).

[8] S.E. Shaheen, C.J. Brabec, N.S. Sariciftci, F. Padinger, T. Fromhertz, J.C. Hummelen "2.5% efficient organic plastic solar cells" *Appl. Phys. Lett.* **78,** 841-43 (2001).

[9] S. Alem, R. de Bettignies, J.-M. Nunzi, M. Cariou, "Efficient polymer-based interpenetrated network photovoltaic cells" *Appl. Phys. Lett.* **84,** 2178-80 (2004).

[10] Kanzan Inoue. Ph.D.Thesis, University of Texas at Dallas, 2006

[11] R. Kline, M. McGehee, E. Kadnikova, J. Liu, J. Frechet, and M. Toney, *Marcromolecules,* **38** (2005) 3312.

[12] Murray, C.B.; Norris, D.J.; Bawendi, M.G. *J. Am. Chem. Soc.* **1993**, *115*, 8706.

[13] Schaller, R.D.; Klimov, 6.2. *Phys. Re6. Lett.* **2004**, *92*, 186601.

[14] Schaller, R.D.; Petruska, M.A.; Klimov, 6.2. *Appl. Phys. Lett.* **2005**, *87*, 253101.

[15] Shockley, W.; Queisser, H. J. *J. Appl. Phys.* **1961**, *32*, 510.

[16] Murray, C.B.; Sun, S.H.; Gaschler, W.; Doyle, H.; Betley, T.A.; Kagan, C.R. *IBM J. Res. De6.* 45, 47 (2001).

[17] Pietryga, J.M.; Schaller, R.D.; Werder, D.; Stewart, M.H.; Klimov, 6.2.; Hollingsworth, J.A. *J. Am. Chem. Soc.* **2004**, *124*, 11752.

[18] Guzelian, A.A.; Banin, U.; Kadavanich, A.6.; Peng, X. ; Alivisatos A.P. *Appl. Phys. Lett.* **1996**, *69*, 1432.
[19] Rogach, A.L.; Harrison, M.T.; Kershaw, S. 6.; Kornowski, A.; Burt, M. G.; Eychmuller, A.; Weller, H. *Phys. Stat. Sol.* **2001**, *224*, 153.
[20] J.M. Pietryga, R.D. Schaller, D. Werder, M.H. Stewart, 6.2. Klimov, J.A. Hollingsworth, "Pushing the Band Gap Envelope:Mid-Infrared Emitting Colloidal PbSe Quantum Dots" *J.Am.Chem.Soc*, **124**, 11752-11753, 2004.
[21] B.L. Wehrenberg, C. Wang, P. Guot-Sionnest, *J. Phys. Chem. B* **106**, 10634, 2002.
[22] Wehrenberg, B.L.; Guyot-Sionnest, P. *J. Am. Chem. Soc.* **2003**, *125*, 7806.
[23] Haram, S.K.; Quinn, B.M.; Bard, A.J. *J. Am. Chem. Soc.* **2001**, *123*, 8860.
[24] Campbell, 2.H.; Hagler, T.W.; Smith, D.L.; Ferraris, J.P. *Phys. Rev. Lett.* **1996**, *76*, 1900.
[25] Liu, Y.; Summers, M.A.; Edder, C.; Frechet, J.M.J.; McGehee, M.D. *Adv. Mater.* **2005**, *17*, 2960.
[26] Schaller, R.D., Agranovich, 6.A.; Klimov, 6.2. *Nat. Phys.* **2005**, *1*, 189.
27 M. Zhang, S. Fang, A.A. Zakhidov, S.B. Lee, A.E. Aliev, C.D. Williams, K.R. Atkinson, R.H. Baughman, "Strong, Transparent, Multifunctional, Carbon Nanotube Sheets", *Science* 309, 1215-1219, 2005. [10] C. L. Pekeris, Phys. Re6. **112**, 1649 (1958); *Phys. Rev.* **126**, 1470 (1962)
[28] A.G. Rinzler and Z. Chen, Transparent electrodes from single wall carbon nanotubes, US2004/0197546 A1; Z.Wu, Z.Chen, Xu Du, J. Logan, et.al., "Transparent, Conductive Carbon Nanotube Films" *Science* **305**, 1273, 2004
[29] M. Kaempgen and S. Roth, Transparent CNT Composites, *AIP Proceedings*, (2003)
[30] N. Saran, K. Parikh, D.-S. Suh, E. Munoz, H. Kolla, and S. Manohar. "Fabrication and characterization of thin films of single-wall carbon nanotube bundles on flexible plastic substrates." *JACS Comm.* **126**, 4462-4463 (2003)]
[31] K. Inoue, R. Ulbricht, P. C. Madakasira, M. Zhou, S. B. Lee, J. Ferraris and A. Zakhidov, "High Efficiency Solar Cells based on Optimally Annealed P3HT/PCBM" Synthetic Metals, *Proc. of MRS 2004*, 6. **836**, L3.2, 2005
[32] K. Hata, D. Futaba, K. Mizuno, T.Namai, M.Yumura and Iijima, *Science* **306** (2004)1362
[33] R. Loewe, R. McCullough, etc. " Regioregular Head-to-Tail Coupled Poly(3-alkylthiophenes) Made Easy by the GRIM Method: Investigation of the Reaction and the Origin of Regioselectivity" *Macromolecules* **34**, 4324 – 4333, 2001.
[34] L. Zhai, R. McCullough,etc. " A Simple Method to Generate Side-Chain Derivatives of Regioregular Polythiophene via the GRIM Metathesis and Post-polmerization Functionalization" *Macromolecules* **36**, 61-64, 2003.
[35] Liu, Jinsong; Tanaka, Toru; Sivula, Kevin; Alivisatos, A. Paul; Frechet, Jean M. J. *JACS* **126**(21), 6550-6551, 2004.
[36] Ferraris, John P.; Yassar, Abderrahim; Loveday, David C.; Hmyene, Mohamed, *Optical Materials*, 9(1-4), 34-42, 1998.
[37] H. Sirringhaus et.al., *Nature*, **401**, 685(1999).
[38] R. Österbacka, C.P. An, X.M. Jiang, and Z.6.Vardeny, *Science*, **287**, 739 (2000)

Personnel supported

- Kanzan Inoue – Graduate Ph.D. Student of UTD, Physics Department
- Ross Ulbricht – Undergraduate Student, of UTD, Physics Department
- Pallavi C. Madakasira – Master Student, of UTD, Physics Department
- William M. Sampson, Graduate Ph.D.student of UTD, Physics Department
- Prof. Anvar Zakhidov's one-month summer salary was supported from the grant
- Dr. Xiaomei Jiang was supported partially by this grant and partially by SPRING Consortium of Texas (also managed by AFOSR)

Publications

1. K. Inoue, R. Ulbricht, P. C. Madakasira, W.M. Sampson, S. Lee, J. Gutierrez, J.P. Ferraris, A.A. Zakhidov, "Optimization of Postproduction Heat Treatment for Plastic Solar Cell", ***Proc. of SPIE – Volume 5520***, Organic Photovoltaics V, 2004, in press.
2. K. Inoue, R. Ulbricht, P. C. Madakasira, W.M. Sampson, S. Lee, A.A. Zakhidov, "Temperature and Time Dependency of Heat Treatment of RR-P3HT/PCBM Plastic Solar Cell", ***Synthetic Metals*** (2005), 154(1-3), 41-44.
3. X. Jiang, S. Lee, Richard D. Schaller, Jeff M. Pietryga, Victor 2. Klimov and A.A. Zakhidov, "Nanocomposite Solar Cells Based on Conjugated Polymer/ PbSe Quantum Dot", ***Proc. Of SPIE***, 5938 (2005), 59381F.
4. X. Jiang, R.D. Schaller, S.B. Lee, J.M. Pietryga, 6.2. Klimov and A.A. Zakhidov (2006). PbSe Nanocrystal/Conducting Polymer Solar Cells with 2 Microns Infrared Response, submitted to ***Adv. Mater.***
5. Zhang, Mei; Fang, Shaoli; Zakhidov, Anvar A.; Lee, Sergey B.; Aliev, Ali E.; Williams, Christopher D.; Atkinson, Ken R.; Baughman, Ray H, "Strong, Transparent, Multifunctional, Carbon Nanotube Sheets", ***Science*** (2005), 309 (5738), 1215-1219.
6. R. Ulbricht, X. Jiang, S.B. Lee, M. Zhang, S. Fang, B.H. Baughman and A. A. Zakhidov, " Polymeric Solar Cells with oriented Strong Transparent Carbon Nanotube Anode, ***Phys. Stat. Sol. B***, 2006 (in press),
7. P. Madakasira, K. Inoue, R. Ulbricht, S.Lee, M. Zhou, J.P. Ferraris and A.A. Zakhidov, "Multilayer encapsulation of plastic photovoltaic devices", ***Synth. Met.***, **155**(2), 332-335,2005.
8. Ross Ulbricht, Sergey B. Lee, Kanzan Inoue, Mei Zhang, Shaoli Fang, Ray H. Baughman and Anvar A. Zakhidov, "Transparent Carbon Nanotube Sheets as 3-D Charge Collectors in Organic Solar Cells", ***Solar Energy Materials & Solar Cells***, 2006 (in press).

Interactions/Transitions

a. Participation/presentations at meetings, conferences:

The results were presented at many international and national conferences:

1. International Conference on Synthetic Metals, Australia, July 2004 and Dublin, 2006 at
2. SPIE Annual Meeting, Denver, Colorado, August 2004.

3. SPIE Annual Meeting, San Diego, CA, August 2005.
4. MRS Fall Meetings, Boston 2003, 2004, 2005
5. MRS Spring meeting, San Francisco, March 2006
6. APS march meetings, 2004, 2005, 2006

b. Based on the results of our research we have interactions with a Solar Cells Lab of the Wright -Patterson Air Force Research Labs. We have prepared a mutual proposal teaming with Dr. Michael Durstock on the polymeric photocells, but proposal was not awarded by DARPA. We are working on preparation of another mutual program.

c. The results of our Work on plastic solar cells with the efficiency of > 3 % are planed to be transferred for the use in same Wright-Patterson Air Force Research Lab to Dr. Michael Durstock of Materials and Manufacturing Directorate.
The copy of present Report and our recent publications are forwarded to Dr. M. Durstock